Global Biogeochemical Cycles

RESEARCH ARTICLE
10.1029/2024GB008387

Fish Carbonates in the North Atlantic and Their Potential Role in the Carbon Cycle

Mohammed S. Hashim[1,2], Maureen H. Conte[3,4], Michael A. Salter[5], Rut Pedrosa-Pamies[4], J. C. Weber[4], Matthew G. Hayden[1], Rod W. Wilson[5], Chris T. Perry[6], Stephen F. Crowley[7], Paul F. Dennis[8], David Bish[9], and Adam V. Subhas[1]

[1]Department of Marine Chemistry and Geochemistry, Woods Hole Oceanographic Institution, Woods Hole, MA, USA, [2]Now at Department of Earth Sciences, University of Southern California, Los Angeles, CA, USA, [3]Bermuda Institute of Ocean Sciences, St. Georges, Bermuda, [4]The Ecosystems Center, Marine Biological Laboratory, Woods Hole, MA, USA, [5]Biosciences, University of Exeter, Exeter, UK, [6]Geography, University of Exeter, Exeter, UK, [7]Department of Earth, Ocean and Ecological Science, University of Liverpool, Liverpool, UK, [8]School of Environmental Sciences, University of East Anglia, Norwich, UK, [9]Department of Chemistry, Indiana University, Bloomington, IN, USA

Key Points:

- We analyzed enigmatic blue particles collected at various depths by sediment traps via the Oceanic Flux Program in the North Atlantic
- We found direct evidence of fish-produced carbonates in the open ocean
- We discuss the formation mechanism of fish carbonates, their abundance, seasonality, and importance to alkalinity and carbon in the ocean

Supporting Information:

Supporting Information may be found in the online version of this article.

Correspondence to:

M. S. Hashim,
Mohammed.hashim@whoi.edu

Citation:

Hashim, M. S., Conte, M. H., Salter, M. A., Pedrosa-Pamies, R., Weber, J. C., Hayden, M. G., et al. (2025). Fish carbonates in the North Atlantic and their potential role in the carbon cycle. *Global Biogeochemical Cycles*, *39*, e2024GB008387. https://doi.org/10.1029/2024GB008387

Received 8 OCT 2024
Accepted 22 MAY 2025

Author Contributions:

Conceptualization: Mohammed S. Hashim, Maureen H. Conte, Adam V. Subhas
Data curation: Mohammed S. Hashim, Maureen H. Conte, Michael A. Salter, Rut Pedrosa-Pamies, J. C. Weber, Matthew G. Hayden, Rod W. Wilson, Chris T. Perry, Stephen F. Crowley, Paul F. Dennis, David Bish
Funding acquisition: Mohammed S. Hashim, Maureen H. Conte, Rut Pedrosa-Pamies, Rod W. Wilson, Chris T. Perry, Adam V. Subhas
Investigation: Mohammed S. Hashim, Maureen H. Conte, Michael A. Salter, Rut Pedrosa-Pamies, Rod W. Wilson, Chris T. Perry, David Bish, Adam V. Subhas
Methodology: Mohammed S. Hashim, David Bish
Project administration: Mohammed S. Hashim
Writing – original draft: Mohammed S. Hashim

Abstract Marine fish precipitate carbonates in their intestines that they subsequently excrete as part of an osmoregulatory strategy. While fish carbonates are proposed to be volumetrically significant to the global carbonate budget, no study has presented direct evidence of fish carbonates in the open ocean. Here we examine sediment trap material collected by the Oceanic Flux Program (OFP) in the North Atlantic and observe the episodic occurrence of enigmatic blue particles since 1992. The blue particles are comprised of calcite with unusually high magnesium content (up to 46 mol%) with distinctively depleted $\delta^{13}C$ and enriched $\delta^{18}O$ compared with calcite produced by common marine calcifiers. Based on the mineralogical, isotopic, and textural similarities between the blue particles and fish carbonates, we propose that the blue particles are produced by pelagic fish. Our data suggest that fish modify their intestinal fluids to create a concentrated, highly supersaturated, ^{13}C depleted solution capable of precipitating calcite with high magnesium content and low $\delta^{13}C$. Collectively, our data imply that fish carbonate production is an open-ocean phenomenon, opening up the possibility that fish contribute to the production, dissolution, and export of carbonates globally.

1. Introduction

Calcium carbonate ($CaCO_3$) minerals in the ocean are an integral part of the global carbon cycle and have significant implications for atmospheric CO_2 concentrations (Berelson et al., 2007; Milliman, 1993; Ridgwell et al., 2003). Despite their significance, estimates of $CaCO_3$ production, export, and dissolution remain poorly constrained (Adkins et al., 2021; Berelson et al., 2007; Milliman & Droxler, 1996). The continued upward revision of total $CaCO_3$ production rates (Knecht et al., 2023; Kwon et al., 2024; Liang et al., 2023) requires a corresponding increase in shallow dissolution in order to close the oceanic $CaCO_3$ budget (Berelson et al., 2007; Sulpis et al., 2021). While recent studies have suggested a bigger role for coccolithophore dissolution in the upper ocean (Dean et al., 2024; Neukermans et al., 2023; Subhas et al., 2022; Ziveri et al., 2023), the contribution from other $CaCO_3$ producers to production, export, and dissolution is an open question (Knecht et al., 2023).

Marine fish precipitate calcium and magnesium carbonates (hereafter fish carbonates) in their intestines that they subsequently excrete to remove accumulated Ca and Mg ions as part of their osmoregulatory strategy (Grosell & Oehlert, 2023; Walsh et al., 1991; Wilson et al., 2002, 2009). Estimates of fish produced carbonates in the ocean vary considerably (Oehlert, Garza, et al., 2024; Wilson et al., 2009). Recent estimates of global fish biomass have increased (Irigoien et al., 2014; Jennings & Collingridge, 2015; Proud et al., 2019), prompting an upward revision of global fish carbonate production to between 0.04 and 1.08 Pg $CaCO_3$-C yr^{-1} (Oehlert, Garza, et al., 2024). If true, $CaCO_3$ production by fish approaches or even exceeds that by pelagic foraminifera (~1.0–1.2 Pg $CaCO_3$-C yr^{-1} (Knecht et al., 2023; Langer, 2008), coccolithophores (~1.0 Pg $CaCO_3$-C yr^{-1} or higher (Broecker & Clark, 2009; Knecht et al., 2023), and coral reefs (0.108 Pg $CaCO_3$-C yr^{-1} (Milliman & Droxler, 1996). Despite the proposed significance of fish produced carbonates for the global carbon cycle, fish production has only been estimated by multiplying fish biomass, which itself is highly variable (e.g., Proud et al., 2019), by carbonate production rates determined experimentally for a few species of neritic fish maintained under controlled laboratory conditions with food withheld (Oehlert, Garza, et al., 2024; Perry et al., 2011; Salter et al., 2012, 2017). Thus far, no study has provided direct evidence of fish-produced carbonates in the open ocean.

Writing – review & editing: Mohammed S. Hashim, Maureen H. Conte, Michael A. Salter, Rut Pedrosa-Pamies, J. C. Weber, Matthew G. Hayden, Rod W. Wilson, Chris T. Perry, Stephen F. Crowley, Paul F. Dennis, David Bish, Adam V. Subhas

Fish produced carbonates exhibit unique morphologies, mineralogical compositions, geochemical signatures, and reactivities relative to more traditional open-ocean $CaCO_3$ sources (Hashim & Kaczmarek, 2019). They are morphologically diverse and include ellipsoids, dumbbells, spheres, and rhombohedra (Perry et al., 2011; Salter et al., 2012). Similarly, the size of the precipitates varies greatly and ranges from <1 to ∼30 μm, though the precipitates typically form aggregates (i.e., excreted pellets) that can measure up to 2,000 μm (Salter et al., 2014). Carbonates produced by >80 fish species have been examined to-date, and among these the dominant mineralogy is most commonly high-Mg calcite (HMC) with a wide range of Mg contents (Oehlert, Garza, et al., 2024; Perry et al., 2011; Salter et al., 2017, 2019), but low-Mg calcite, aragonite, monohydrocalcite, and amorphous $CaCO_3$ have also been reported (Perry et al., 2011; Salter et al., 2018).

Calcite solubility is a function of Mg content, whereby solubility decreases to a minimum value at $MgCO_3$ of 4 mol% followed by a general increase with increasing Mg content (Morse et al., 2006). As such, most fish carbonates, which generally have high Mg contents, are considered to be highly soluble. It is important to note that only one study (Woosley et al., 2012) measured the solubility of fish carbonates and used fish precipitate with 47.9 mol% $MgCO_3$. Furthermore, the solubility of carbonate minerals is influenced by crystallinity, lattice strain, and cation disorder in addition to Mg content (Bischoff et al., 1987; Morse et al., 2006). Given that fish carbonates are mineralogically heterogenous and characterized by a wide range of Mg contents, it is likely that fish carbonates exhibit a wide range of solubilities. The dissolution of the highly soluble fish produced carbonates could help to reconcile the long-standing gap in the marine $CaCO_3$ and alkalinity budgets, especially in the upper ocean (Wilson et al., 2009). However, the packaging into larger aggregates, often with organic coatings (Oehlert, Arista, et al., 2024), also suggests that fish-produced carbonates could sink rapidly before disaggregation and contribute to deeper export of carbonates and organic carbon (Oehlert, Garza, et al., 2024).

The Oceanic Flux Program (OFP) time series has continuously measured particle fluxes in the Sargasso Sea since 1978 using sediment traps located at 500, 1,500, and 3,200 m water depths (Conte et al., 2001, 2025), providing a unique opportunity to assess the sources and sinks of carbonates in the North Atlantic water column. In the mid 1990s, enigmatic greenish blue macroaggregates (hereafter "blue particles") of unknown origin were first noted in the OFP traps (Ralph et al., 1998). The macroaggregates, ranging in size from a few hundred micrometers to several millimeters, surprisingly were found to consist almost exclusively of sub-micrometer size particles of magnesian calcite, with only minimal quantities of typical pelagic carbonate particles embedded within the calcite matrix (Figure 1). Blue particles have continued to be found sporadically in the OFP sediment traps, primarily at 500 m depth in the winter and spring (Table 1), but the mystery of their origin(s) has never been solved.

Here, we tested the hypothesis that the enigmatic blue particles are produced by pelagic fish, and if so, could represent an important source of soluble carbonate in the open ocean. We test this hypothesis by conducting a suite of analyses on these blue particles to assess their mineralogy, elemental and isotopic compositions, and morphological characteristics. We contrast the blue particle composition with that of the particulate carbonate flux at the OFP site and with pelagic carbonate producers (foraminifera, pteropods, coccolithophores, and bryozoan and serpulid worm epiphytes on *Sargassum*). We also compare the morphology and carbonate composition of the blue particles with the carbonate produced by several species of neritic bony fish.

2. Methods

2.1. Sampling Sites and Processing

All samples used in this study can be found in archived data sets (Hashim et al., 2025a, 2025b) and are described in detail in the following sections. We analyzed several samples from the Oceanic Flux Program (OFP) that contain blue particles. For comparison, we analyzed several fish carbonates produced by various neritic fish species. We also analyzed a selected number of bulk OFP trap samples from 500, 1,500, and 3,200 m, focusing on the <125 μm size fraction, which comprises most of the total carbonate flux. We also compiled previously published isotopic data on biogenic carbonate producers collected from the OFP traps. These include seasonal isotopic data on dominant pteropod species (e.g., *Limacina inflata and Styliola subula*) in the particle flux (Fabry & Deuser, 1991; Gray, 2019; Jasper & Deuser, 1993; Juranek et al., 2003), and seasonal isotopic data on the major foraminifera species (Babila et al., 2014; Deuser & Ross, 1989; Deuser et al., 1981; Steiger, 2019). We also consider the isotopic composition of coccoliths from *Emiliania huxleyi* coccolithophore cultured in media with known isotopic composition (Hermoso et al., 2014). Additionally, for comparison with neritic carbonate sources on the Bermuda Platform, we included the mineralogy and isotopic composition of resuspended neritic detrital

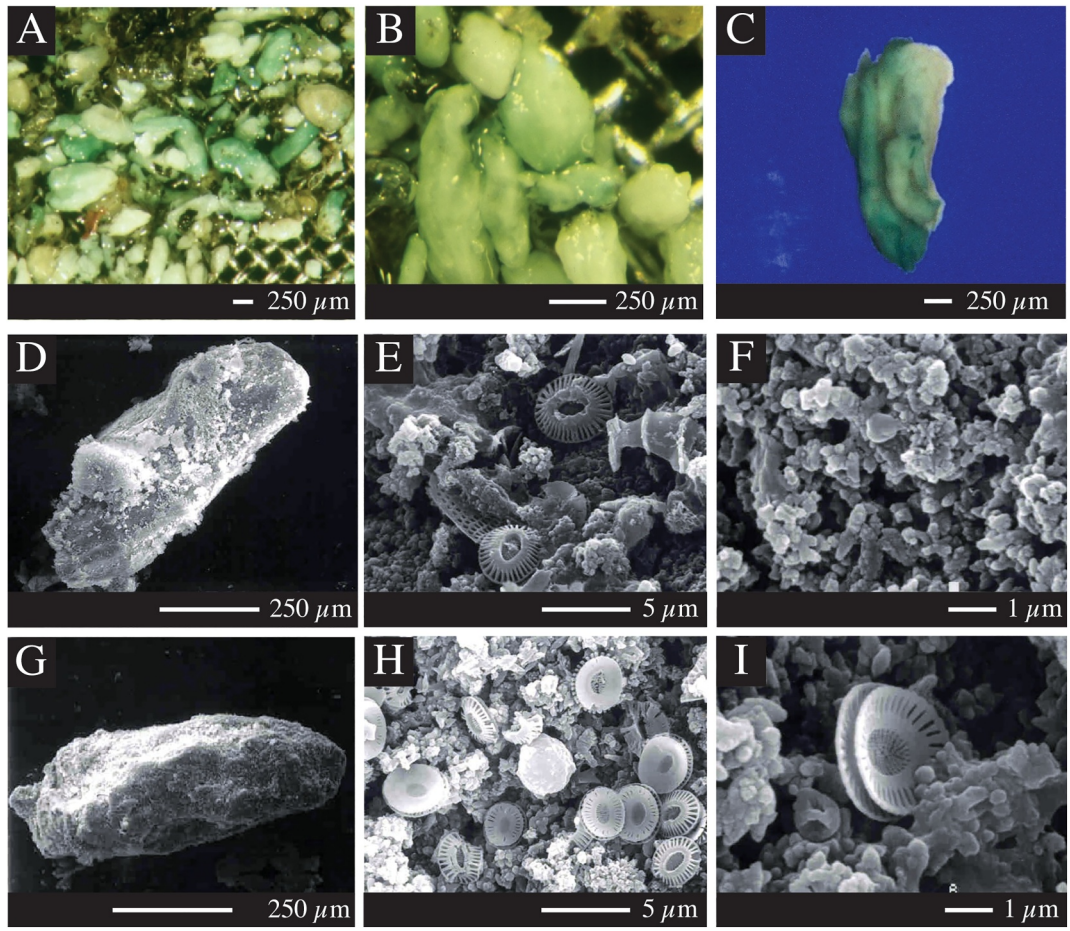

Figure 1. Blue particle aggregates collected in the OFP sediment traps. (a, b) Blue particle aggregates collected 6–23 January 1996 at 500 m depth. (c) Microphotograph of particle collected 14–29 December 2018 at 500 m depth (d–f) SEM images of a blue particle aggregate collected 17 November–2 December 1993 at 500 m depth and closeups of its internal structure of sub-micron sized spherical crystallites with embedded coccoliths and diatom fragments. (g–i) SEM images of a blue particle aggregate collected 9–25 May 1994 at 500 m depth with similar external morphology and internal structure as the particle in (d). The closeup images in (e, f, h, and i) were taken of a broken surface to show the particle interior.

carbonates in the traps that were resuspended on the Bermuda Pedestal and advected to the OFP site during two hurricane events (Pedrosa-Pamies et al., 2025).

2.1.1. The Oceanic Flux Program (OFP) Samples

The Oceanic Flux Program (OFP, 1978–present) time series of the deep ocean particle flux in the oligotrophic deep waters of the subtropical western North Atlantic gyre is the longest and most continuous deep ocean time series in the world (Conte et al., 2025). The OFP mooring site is located in the abyssal plain about 75 km SE of Bermuda in 4,500 m water depth. The area hosts several other long term measurement programs, including the ship-based Bermuda Atlantic Time Series (BATS) of upper ocean biogeochemistry (Lomas et al., 2013).

The OFP sample collection and processing protocols have been described in detail in previous studies (e.g., Conte et al., 2001, 2025). Briefly, three 0.5 m^2 PARFLUX Mark 8 sediment traps (McLane Labs, Falmouth, MA) having a programmable, rotating sampling carousel are affixed to the OFP mooring at depths of 500, 1,500 and 3,200 m and continuously sample the sinking particle flux at a nominal biweekly integration period. Sample collection bottles affixed to the carousel are low density polyethylene (LDPE) and filled with seawater brine of ~40 $g.kg^{-1}$ (40‰) poisoned with ultra-high purity mercuric chloride at a concentration of 0.74 $mmol.L^{-1}$. After recovery, samples are refrigerated at 4°C until processing. Samples are fractionated into four size fractions (>1,000, 500–1,000, 125–500, and <125 μm). Swimmers (live zooplankton and small fish that swim into the sample bottle) are

Table 1
OFP Sediment Trap Samples Since 1992 That Have Contained Blue Particle Aggregates

Sample ID	Mid-date (Days sampling)	Depth (m)	# of aggregates
OFP 4/93-2	26 December 1992 (15)	500	101
OFP 1/94-4	24 November 1993 (13)	500	35
OFP 5/94-8	16 May 1994 (15)	500	23
OFP 1/95-3	22 December 1994 (17)	500	100
OFP 1/95-4	08 January 1995 (18)	500	5
OFP 1/96-4	15 January 1996 (17)	500	4
OFP 1/01-6	11 December 2000 (14)	3,200	35
OFP 4/05-3	10 December 2005 (15)	500	931
OFP 4/06-5	26 January 2006 (15)	500	23
OFP 4/06-6	11 February 2006 (16)	500	20
OFP 4/06-8	15 March 2006 (15)	500	11
OFP 4/06-10	14 April 2006 (14)	500	23
OFP 4/19-3	06 December 2018 (15)	500	~2,640
OFP 4/19-4	21 December 2018 (15)	500	~2,620

removed under a stereomicroscope. The larger size fractions are quantitatively photographed (Conte et al., 2025; Shatova et al., 2012) and then dried at 55°C and weighed with 0.01 mg accuracy. Fish contamination sometimes affects the 500 m trap, with approximately 14.5% of samples containing fish debris (partially decayed fish, fish bones, and scales). In contrast, <1% of 1,500 m and 3,200 m trap samples are contaminated by fish debris.

Samples noted to contain blue particles (Table 1) were targeted for various analyses in this study. Most of the blue particle containing samples were processed and dried as described above. The blue particles in dried samples, identified based on color, shape, and size, were picked using a brush wetted with ethanol under a dissecting microscope. Additionally, in a few samples the blue particle aggregates were picked out during processing and preserved in the trap collection brine. These blue particles were briefly rinsed with MilliQ water and then dried for analysis.

2.1.2. Fish Carbonate

Fish carbonate samples were collected from Eleuthera, The Bahamas, in 2009, 2010, 2011, and 2014, and Lizard Island, Great Barrier Reef, QLD, Australia in 2016 (Hashim et al., 2025b). Additional samples used for visual comparison to blue particles (Figure 3) were collected from Heron Island Research Station and Moreton Bay Research Station, QLD, Australia in 2014 and 2015, and the University of Exeter's Aquatic Resources Center, UK in 2024. At the first three locations, wild fish were collected from the local nearshore environments and housed in aquaria supplied with seawater filtered to 1 μm and maintained close to local ambient conditions (temperature = 24 to 32°C; salinity = 35 to 37; pH_{NBS} = 8.09 to 8.18). At the University of Exeter, commercially sourced fish (gilthead sea bream, *Sparus aurata*) were housed in seawater aquaria maintained at species-appropriate environmental conditions (temperature = 19°C; salinity = 35; pH_{NBS} = 8.00 to 8.10). Food was withheld from fish during the sampling periods, and for 48 hr prior to allow the gastro-intestinal tract to be completely emptied of dietary items and faeces. Excreted carbonates were collected at 24 hr intervals using a plastic Pasteur pipette and were immediately rinsed for a few minutes with distilled water before being immersed in sodium hypochlorite (<5% w/v) for at least 6 hr to remove organic matter. The samples were then rinsed several times with distilled water before being transferred to 0.45 μm filters and dried at 50°C.

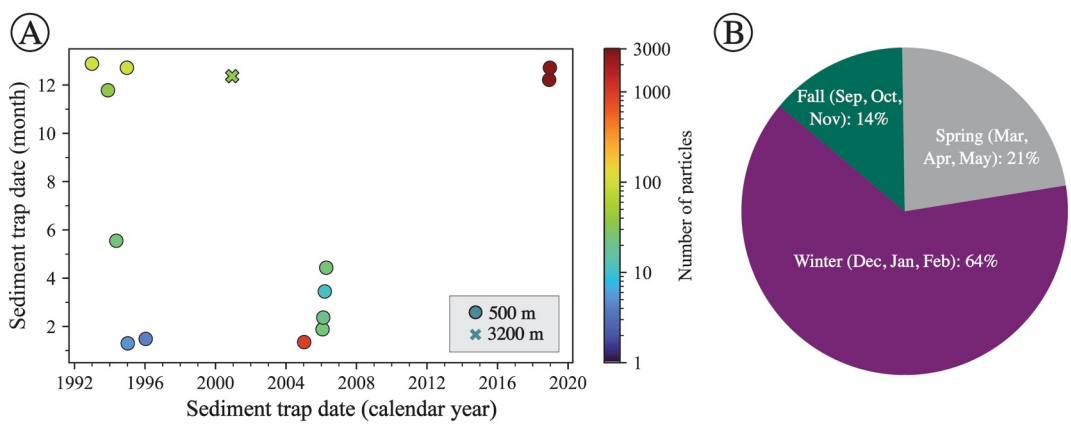

Figure 2. (a) Cross plot between the sediment trap date in calendar years versus the sediment trap date in month of the year color coded by the relative abundance of the blue particles in the sediment trap sample. The plotted date is the middle date between the sediment trap deployment and recovery (Sediment collection period for the plotted samples ranges between 13 and 18 days). The colors represent the number of blue particles in each sample. (b) Pie chart showing the seasons during which the sediment trap that collected the blue particles was deployed and recovered (all samples' deployment and recovery dates fall within the same season). Note that the proportion of samples containing blue particles in the summer is 0% and hence not plotted.

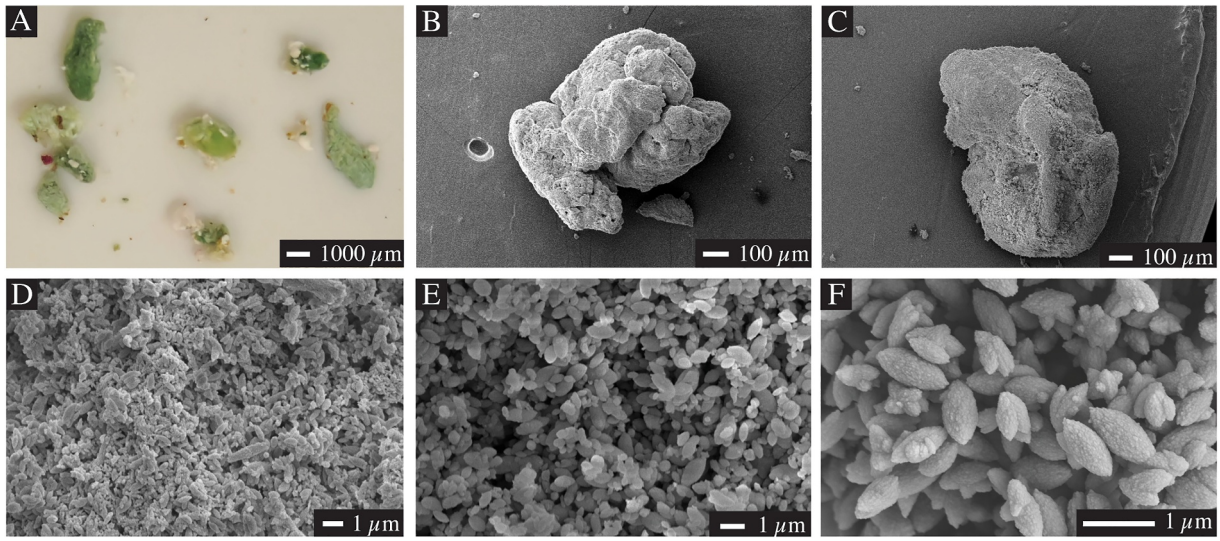

Figure 3. (a) Photograph of untreated fish carbonate pellets excreted by gilthead sea bream (*Sparus aurata*). (b, c) SEM images of a bleach-treated fish carbonate pellet excreted by Moses perch (*Lutjanus russellii*). (d–f) SEM images of bleach-treated fish carbonate pellets showing typical ellipsoidal particles produced by (d) Northern whiting (*Sillago sihama*), (e) Eastern fortescue (*Centropogon australis*), and (f) Spanish flag snapper (*Lutjanus carponotatus*). All fish samples were collected from fasted fish under laboratory conditions at the University of Exeter, UK (a), Moreton Bay Research Station, Australia (b, c, e), Heron Island Research Station, Australia (d), and Lizard Island Research Station, Australia (f). Seawater temperatures ranged from 19 to 30°C and salinity from 35 to 36 PSU. See Salter et al. (2018) for details of sampling conditions at Moreton Bay and Heron Island.

Samples collected in The Bahamas and Australia were primarily obtained from fish that had only ever consumed a mixed diet prior to their collection. However, several individuals of three species sampled in The Bahamas in 2011 (*Lutjanus apodus*, *Albula vulpes*, *and Sphoeroides testudineus*) were provided a diet of sardines (*Sardinella aurita*; Cap'n Salty, Raffield Fisheries Inc., Port St. Joe, FL; sourced from the Gulf of Mexico) for at least 2 weeks prior to carbonates being collected as normal (i.e., fish at fasting state). The isotopic values of carbonates from those fishes are plotted in Figure 5 and referred to as "sardine fed," whereas the rest are referred to as "mixed diet."

2.1.3. Bryozoa, Serpulid Worm, and Coccolithophore

Bryozoa (*Membranipora tuberculata*) and serpulid worm (*Neodexiospira*) epiphytes were isolated from floating *Sargassum* near the OFP site collected on two cruises. *Sargassum* was collected from three sites on an expedition on the R/V *Thomas G. Thompson* from 20 April to 6 May 2021 and at one site on an expedition on the R/V *Atlantic Explorer* in July 2023 (Hashim et al., 2025b). *Sargassum* samples were dried at room temperature and stored in plastic bags. Either a razor blade was used to scrape off attached bryozoans and serpulid tubes (Figure S1 in Supporting Information S1) or bryozoans were removed by gently rubbing dried *Sargassum* fronds with gloved fingers. The separated materials were sieved to remove broken *Sargassum* pieces, soaked in sodium hypochlorite (commercial bleach; 10% w/v) for 24 hr, rinsed with DI water, and dried at 60°C overnight.

Coccolith calcite was obtained from *E. huxlei* coccolithophore (strain #374) cultured at 18°C in a log growth phase with a culture density of $\sim 10^5$ cells/ml. The culture was centrifuged three times at 3,000 rpm for 10 min each. The supernatant was then decanted, and 25 ml of sodium hypochlorite (commercial bleach; 10% w/v) was added. After 24 hr, the sample was filtered through a 0.2 μm polycarbonate filter, which was rinsed with DI water and dried at 60°C overnight. The powder was then scraped into a glass vial and analyzed with X-ray diffraction. This sample was only analyzed for mineralogy. The isotopic values of coccolithophores (Table 2, Figure 5; Hashim et al., 2025c) are sourced from Hermoso et al. (2014).

Table 2
Calcite Mg Content and Inorganic Isotopic Compositions of the Major Sample Types

Sample type	Calcite Mg content mol% (min - max, mean ± 1σ (n))	$\delta^{13}C$ ‰ mean ± 1σ (n)	$\delta^{18}O$ ‰ m ± 1σ (n)	Source of isotopic data
Blue particles	17–46, 32 ± 10 (7)	−2.4 ± 0.7 (22)	2.6 ± 0.6 (15)	This study
Fish	0.27–39, 15 ± 13 (7)	−1.8 ± 1.9 (66)	0.9 ± 0.8 (59)	This study and Pedrosa-Pamies et al. (2025)
OFP carbonate flux (500 m)	0–17, 16 ± 1.6 (6)	0.38 ± 0.42 (12)	0.22 ± 0.3 (12)	This study and Pedrosa-Pamies et al. (2025)
OFP carbonate flux (1,500 m)	0–15, 13 ± 0.9 (12)	0.29 ± 0.42 (18)	0.20 ± 0.3 (13)	This study and Pedrosa-Pamies et al. (2025)
OFP carbonate flux (3,200 m)	0–15, 13 ± 0.8 (13)	−0.43 ± 2.45 (20)	1.44 ± 1.5 (14)	This study and Pedrosa-Pamies et al. (2025)
OFP neritic detrital carbonate (500 m)	n.d.	1.77 (1)[a]	−0.44 (1)[a]	Pedrosa-Pamies et al. (2025)
OFP neritic detrital carbonate (1,500 m)	14.1[a] (a)	1.49 (1)[a]	−0.59 (1)[a]	Pedrosa-Pamies et al. (2025)
Coccolithophores	0 (4)[a]	−1.1 ± 2.9 (10)	0.6 ± 1.5 (10)	Hermoso et al. (2014)
OFP Foraminifera	n.d.	0.08 ± 0.7 (152)	−0.6 ± 0.7 (136)	Deuser and Ross (1989), Deuser et al. (1981), Babila et al. (2014), Steiger (2019)
OFP Pteropods	n.d.	0.7 ± 0.5 (199)	−1 ± 0.5 (199)	Jasper and Deuser (1993), Fabry and Deuser (1992), Gray (2019)
Bryozoan (epiphyte on Sargassum)	17 (1)[a]	−2.1 ± 0.2 (12)	−0.7 ± 0.3 (5)	This study
Serpulid (epiphyte on Sargassum)	18 (1)[a]	1 ± 0.1 (2)	−0.4 (1)[a]	This study
Red Algae	24 (1)[a]	−3.7 ± 0.1 (2)	−5.4 (1)[a]	This study

[a]only mean or mean and number of analyses are reported.

2.2. Analyses

2.2.1. Imaging

As part of the initial OFP analyses in the mid-1990s, blue particles were photographed wet on the stainless sieve and then oven dried at 55°C for analyses. SEM imaging of blue particles was conducted on a JEOL JSM-820 instrument at the University of Massachusetts Dartmouth (Ralph et al., 1998). Samples were gold coated to decrease charging effects. Blue particles in the later OFP samples were quantitatively photographed under a dissecting microscope using methods described in Shatova et al. (2012) before oven drying at 55°C. For some samples, selected blue particles were removed by pipette and archived in the trap brine solution for further analysis.

2.2.2. X-Ray Diffraction (XRD)

XRD was used to determine the mineralogy of samples and to estimate the Mg content (as mol% $MgCO_3$) of calcite. XRD was chosen because it is a nondestructive technique, thus allowing us to subsequently use the same sample for other analyses. This was important given the limited amount of sample available. Beyond this, XRD is a mineralogical approach capable of identifying sample mineralogy and providing individual mineral abundances, making it an ideal technique to characterize the blue particles and other end members and to quantify the

proportion of different phases in the OFP sediment traps. That said, one limitation of XRD is that it is not suitable for quantifying amorphous phases which might be present in our samples. Samples were prepared by gentle powdering using an agate mortar and pestle under acetone. Powders (~20 mg) were then sprinkled onto a silicon zero-background diffraction plate and flattened with a glass slide (Hashim et al., 2023; Hashim & Kaczmarek, 2020). The plate was then placed in an automatic sample changer. Measurements were conducted at the MIT.nano facility using a PANalytical X'Pert PRO X-ray powder diffractometer using a Cu anode and an X'Celerator Scientific 1D position-sensitive detector in Bragg-Brentano geometry. XRD data were collected from 5 to 100° 2θ with a count time of 1 s/step and were processed using the fundamental-parameters Rietveld refinement software TOPAS V7 (Bruker, AXS, Karlsruhe, Germany). The data were corrected for an instrument zero error of -0.09 ± 0.001 determined using the NIST standard LaB_6 (660c), which has a certified unit-cell parameter of 4.156826 Å, crystallite size of 500 nm, and no micro-strain related peak broadening (Black et al., 2020). Instrument parameters were set to known values during Rietveld refinement and a specimen displacement correction was refined for every sample. TOPAS was used to determine relative mineral abundances, unit-cell parameters, crystallite size, and micro-strain (Bish & Howard, 1988). Preferred orientation was modeled using the March-Dollase model. TOPAS provided a set of parameters that include relative abundances (%) of all phases in the sample, their unit-cell parameters (a and c for calcite), crystallite size, and micro-strain for each phase. The Mg content of calcite phases expressed as mol% $MgCO_3$ was determined using the refined a unit-cell parameter based on the empirical relationship of Zhang et al. (2010) between calcite unit-cell parameters and its $MgCO_3$. All raw XRD data along with Rietveld-derived wt.% calcite and mol% $MgCO_3$ values for each sample are provided by Hashim et al. (2025d). There are two sources of uncertainty associated with these parameters. The first is related to the Rietveld refinement results for both mineral wt.% and unit-cell parameters, which were used to derive the Mg content. The Rietveld-determined wt.% error for each phase for each sample is always <3% for mineral abundances, which are reported as a percentage. The error of the unit-cell parameters that is reported by TOPAS (Coelho, 2018) translates to a maximum of 0.7 mol% $MgCO_3$. The second source of uncertainty impacting mol% $MgCO_3$ is from the relationship between the a unit-cell parameter and $MgCO_3$ (Zhang et al., 2010), which is estimated to be <2 mol%.

2.2.3. Electron Microprobe (EMPA)

EMPA data were collected for bulk OFP samples (<125 μm size fraction) and a blue particle sample using a JEOL JXA-8530F electron microprobe, equipped with five wavelength-dispersive spectrometers (WDS) and a SiLi energy-dispersive spectrometer (EDS). Measurements were done on carbon-coated thin sections. Analytical conditions were 15 kV accelerating voltage, a 7–10 nA beam current, and beam spot sizes of 5–21 μm. X-ray intensities were referenced to carbonate, silicate, phosphate, or sulfate standards, with phi-rho-Z matrix corrections applied. Stoichiometric oxygen was assigned to the calculated cationic concentrations for matrix-correction calculations and oxide-format display. Matrix-correction calculations converged within 6–10 iterations. In total, 64 spots were analyzed in addition to the high-resolution map shown in Figure 4. Of the spots analyzed, 15 were conducted on a bulk OFP sample from 500 m, 3 on a bulk OFP sample from 1,500 m, 6 on a bulk OFP sample from 3,200 m, and 6 on a blue particle sample. All these data are plotted in Figure 9.

2.2.4. Stable Carbon and Oxygen Isotopic Analysis

Isotopic compositions ($\delta^{13}C$ and $\delta^{18}O$) of blue particles and other biogenic carbonates recovered from OFP traps were either measured in this study or taken from published sources (Hashim et al., 2025c). All new analyses were undertaken using local versions of the classical phosphoric acid decomposition method used to prepare pure CO_2 for isotope ratio measurement (McCrea, 1950). Initial $\delta^{13}C$ and $\delta^{18}O$ analyses of blue particles and biogenic carbonate were conducted at the WHOI mass spectrometry facility using a Finnigan MAT 252 isotope ratio mass spectrometer (IRMS) attached to a Kiel I carbonate device (Ostermann & Curry, 2000). The second group of measurements ($\delta^{13}C$ only) were conducted by cavity ring-down infrared spectroscopy using a Picarro DIC and $\delta^{13}C$-DIC analyzer in the Subhas Laboratory at WHOI (Su et al., 2019; Subhas et al., 2019). The third group of measurements (both $\delta^{13}C$ and $\delta^{18}O$) were conducted using a Finnigan MAT 253 Plus dual inlet IRMS linked to a Kiel IV carbonate device at Brown University. All sample analyses were calibrated against local secondary laboratory reference materials with compositions defined by measurement against the NBS19 international reference material and the respective isotope ratios reported relative to the Vienna Pee Dee Belemnite (VPDB) international reference scale.

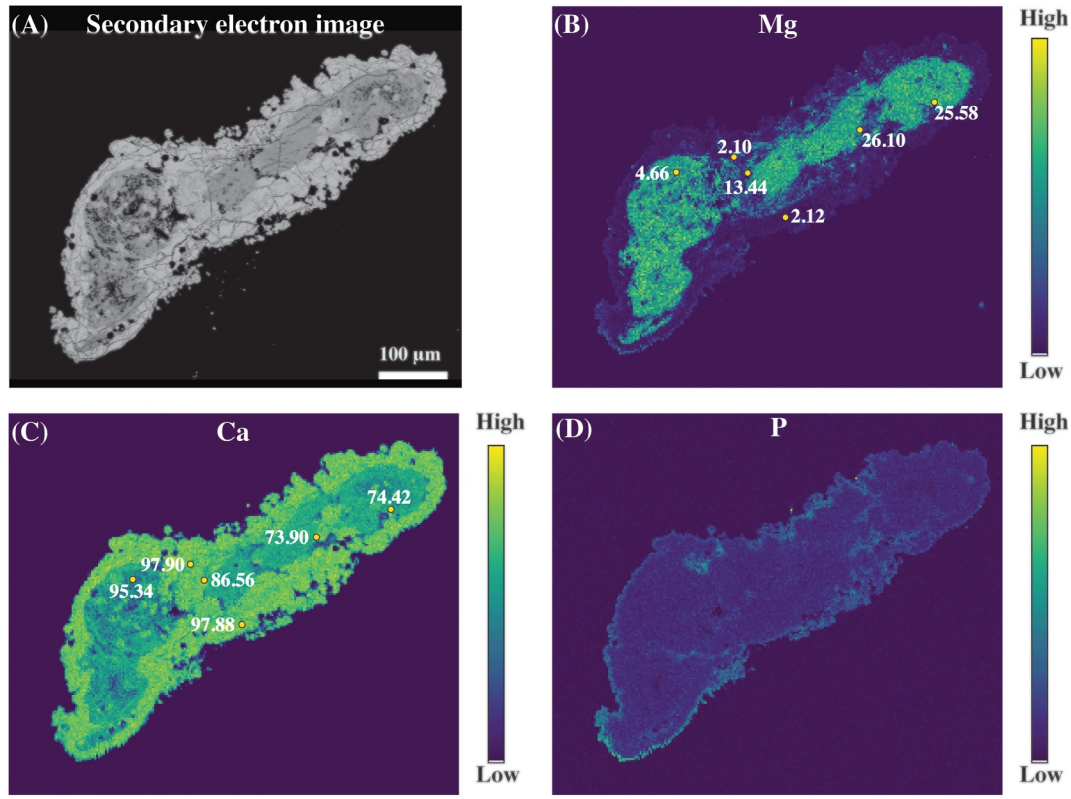

Figure 4. Electron microprobe elemental data for a blue particle from sample OFP 4/19-4 500 m. (a) A secondary electron image showing the blue particle. (b) A map of the blue particle Mg content in x-ray counts. The yellow circles represent spot analysis showing the Mg content in mol%. (c) A map of the blue particle Ca content in x-ray counts with the yellow circles showing the Ca content in mol%. (d) A map of phosphorous for the blue particle with notable rim of high phosphorous content.

Isotopic analysis of fish carbonates ($\delta^{13}C$ and $\delta^{18}O$) was conducted at the University of Liverpool (2–3 mg-sized samples) using VG SIRA10 a dual-inlet IRMS, and at the University of East Anglia (50–80 mg-sized samples) using a modified VG dual-inlet SIRA series II IRMS. All sample analyses were calibrated with respect to VPDB via contiguous measurement of local secondary laboratory reference materials with compositions defined against international reference materials NBS18 and NBS19. Analytical precision for carbon and oxygen isotope ratios measured at both laboratories is estimated to be better than ±0.1 ‰ (1σ) based on replicate analysis of laboratory quality control materials and selected fish carbonate samples.

The $\delta^{13}C$ of DIC of seawater samples collected at the BATS site during an expedition in July 2023 were measured using an Apollo-Picarro CO_2 analyzer (Subhas et al., 2022). All analyses were standardized against certified reference materials and an in-house laboratory standard made from seawater obtained from the Environmental Systems Laboratory at WHOI. The seawater samples were collected using Niskin bottles and poisoned $HgCl_2$ according to established methods (Dickson et al., 2007). These data are presented in Table S1 in Supporting Information S1.

2.3. Calculations

The saturation state (Ω) with respect to fish carbonates (Figure S4 in Supporting Information S1) was calculated via Ocean Data View (Schlitzer, 2022) using the Bermuda Atlantic Time Series (BATS) bottle data (Lomas et al., 2013). First, we calculated Ω with respect to aragonite using the DIC and alkalinity pairs and the equilibrium constants from the Best Practices Handbook 2007. We then calculated the Ω with respect to fish carbonates using the following equation:

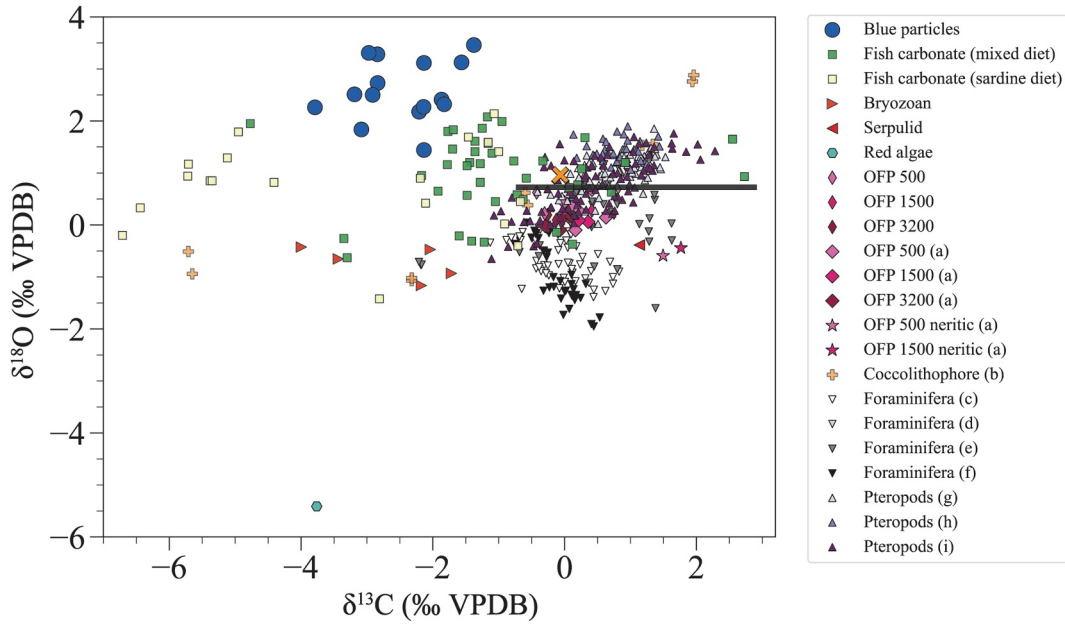

Figure 5. Cross plot between $\delta^{13}C$ and $\delta^{18}O$ of the blue particles, bulk Oceanic Flux Program (OFP) carbonate, foraminifera and pteropods collected in the OFP traps and additionally plumes of detrital neritic carbonate sediments from the Bermuda Platform advected to the OFP site during two hurricane events (see text), coccoliths, bryozoan, serpulid, and red algae. The horizontal gray line represents the $\delta^{13}C$ range of seawater at the nearby BATS site estimated using measured $\delta^{13}C$ (Table S1 in Supporting Information S1) and data from Brooks (2020). The orange x symbol represents the isotopic composition of the coccolithophore culture media (Hermoso et al., 2014). Letters in the legend refer to data sources. (a) Pedrosa-Pamies et al. (2025); (b) Hermoso et al. (2014); (c) Deuser and Ross (1989); (d) Deuser et al. (1981); (e) Babila et al. (2014); (f) Steiger (2019); (g) Jasper and Deuser (1993); (h) Fabry and Deuser (1992); (i) Gray (2019). The uncertainty in the measurements (1) is smaller than the size of symbols.

$$\Omega_{\text{fish\_carb}} = \frac{\Omega_{\text{arag}} * K^*_{\text{sp,arag}}}{K^*_{\text{sp,fish\_carb}}} \quad (1)$$

Where $\Omega_{\text{fish\_carb}}$ and Ω_{arag} are the saturation state with respect to fish carbonate and aragonite, respectively, and $K^*_{\text{sp,arag}}$ and $K^*_{\text{sp,fish\_carb}}$ are the apparent solubility in seawater of aragonite (Mucci, 1983) and fish carbonate with 47.9 mol% $MgCO_3$ (Woosley et al., 2012), respectively. It should be noted that the calculated Ω with respect to fish carbonate is highly uncertain given that K_{sp} for fish carbonate is only known for material with ~48 mol% $MgCO_3$, yet we observed a wide range of Mg contents in the blue particles and fish carbonates.

Seawater temperature, salinity, and Ω_{calcite} from the BATS bottle data were plotted against the blue particle Mg content, $\delta^{13}C$, and $\delta^{18}O$ (Figures S7 and S8 in Supporting Information S1). This was done by filtering the data to include only the upper 50 m of the water column where the seasonal variability in temperature, salinity, and Ω_{calcite} is apparent (Figure S7 in Supporting Information S1). A curve was fitted between each of temperature, salinity, and Ω_{calcite} and month of year using the piece-wise linear least-squares function with 20 grid points in ODV (Figure S7 in Supporting Information S1).

Salinity from BATS in the upper 500 m of the water column was used to calculate $\delta^{18}O$ of seawater ($\delta^{18}O_{sw}$) using the empirical equation of Juranek et al. (2003):

$$\delta^{18}O_{sw} = 0.538 * S - 18.6 \quad (2)$$

Where $\delta^{18}O_{sw}$ is the oxygen isotope of seawater in per mil (VSMOW) and S is salinity in PSU. $\delta^{18}O_{sw}$ was converted from VSMOW to VPDB using the following equation (Brand et al., 2014):

$$\delta^{18}O_{sw}(\text{VPDB}) = 0.97001 * \delta^{18}O_{sw}(\text{VSMOW}) - 29.99‰ \quad (3)$$

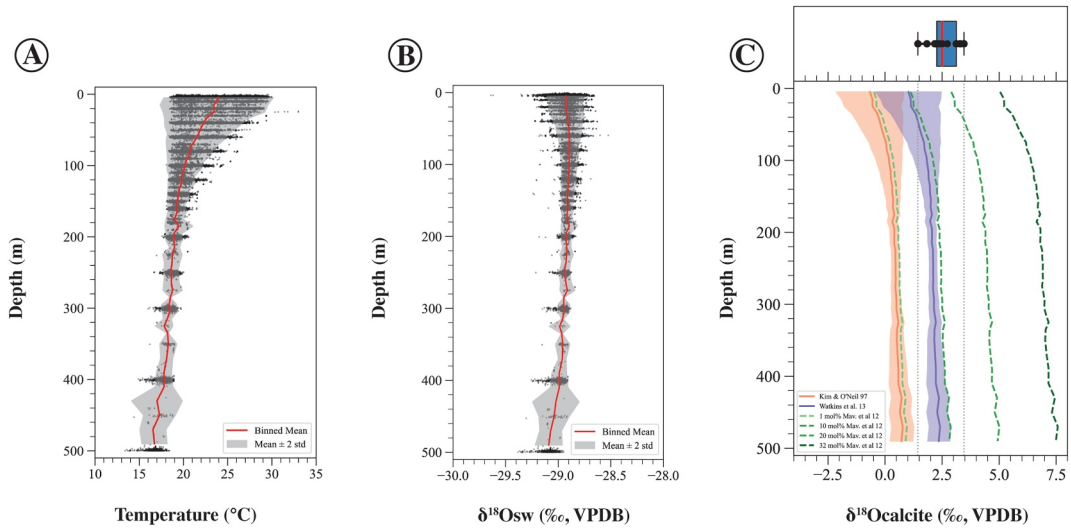

Figure 6. (a) Seawater temperature in the upper 500 m of the water column at the BATS site with the mean (red line) calculated for binned data within 10 m depth window between 0 and 340 and 20 m depth window for >340 m. The shaded area is 2σ around the mean also calculated for binned data. (b) $\delta^{18}O$ of seawater calculated from salinity (see text for details) with binned mean and 2σ using same binning intervals as temperature. (c) $\delta^{18}O$ of calcite calculated using the $\delta^{18}Osw$ of seawater at each depth and the fractionation factor of Kim and O'Neil (1997) (orange solid), Watkins et al. (2013) (purple solid) corrected for temperature from each depth as well as the fractionation factor of Mavromatis et al. (2012) (green dashed) corrected for temperature from each depth and using different $MgCO_3$ in calcite (1, 10, 20, and 32 mol% Mg). The shaded areas were determined by propagating the error from $\delta^{18}Osw$ and temperature (see text for details). The box and whisker plot represents the $\delta^{18}O$ of the blue particles and the dotted vertical lines represent the min and max of the blue particle $\delta^{18}O$.

The mean and standard deviation (**σ**) of $\delta^{18}O_{sw}$ (Figure 6a) and seawater temperature (Figure 6b) were calculated by binning data within 10 m bins between 0 and 340 and 20 m bins between 340 and 500 m of the water column. Thicker bins were used for the deeper interval due to the paucity of the data (Figures 6a and 6b). Temperature was used to calculate the equilibrium oxygen fractionation factor (α) using equations from Kim and O'Neil (1997) and Watkins et al. (2013) in the following form:

$$1000 \ln \ln \alpha = A * \frac{1000}{T} + B \tag{4}$$

where T is in Kelvin. The equations of Kim and O'Neil (1997) and Watkins et al. (2013) were used because they are believed to represent kinetic (Kim & O'Neil, 1997) and equilibrium (Watkins et al., 2013) fractionation factors (Dietzel et al., 2009; Watkins et al., 2013, 2014). In addition, we calculated $1000\ln(\alpha)$ based on the empirical equation of Mavromatis et al. (2012), which relates $1000\ln(\alpha)$ to temperature and the $MgCO_3$ of calcite. This was done using seawater temperature (Figure 6a) and $MgCO_3$ of 1, 10, 20, and 32 mol%. Note that using an $MgCO_3$ value of 0 mol% produces a curve identical to that of Kim and O'Neil (1997).

To incorporate the observed range of seawater temperature (i.e., seasonal variability) in the calculation of 1000lnα that used the equations of Kim and O'Neil (1997) and Watkins et al. (2013), we used the first-order Taylor expansion approach (Bevington & Robinson, 2003) by calculating the first derivative of 1000lnα:

$$\frac{f(T)}{dT} = -A * \frac{1000}{T^2} \tag{5}$$

Where $f(T)$ is the $1000\ln(\alpha)$ which is a function of T as shown in Equation 4. The $f(T)$ was then multiplied by the standard deviation of temperature of each bin (σ_T) to obtain the uncertainty of $1000\ln(\alpha)$ due to temperature variability. We used the following equation to propagate the variability of both $1000\ln\alpha$ (due to temperature) and $\delta^{18}O_{sw}$:

$$\sigma_{\delta^{18}O_{cal}} = 2 \times \sigma_T + 2 \times \sigma_{\delta^{18}O_{sw}} \quad (6)$$

Where $\sigma_{\delta^{18}O_{cal}}$ is the uncertainty in the $\delta^{18}O_{calcite}$, which is plotted as a shading area in Figure 6c and $\sigma_{\delta^{18}O_{sw}}$ is the standard deviation of $\delta^{18}O_{sw}$.

3. Results

3.1. Occurrence in the OFP Traps

While the OFP sediment traps collect continuously, blue particles have only been observed in 14 trap samples since 1992 (Table 1 and Figure 2). All samples having blue particles were from traps sampling at 500 m depth, except one from 3,200 m depth and were only observed in traps sampling between November and May. Blue particle abundance in the samples varied widely, from <10 to >2,500 aggregates with no systematic seasonal or interannual variation in abundance ($p >> 0.05$).

3.2. Morphology

The blue particles, although generally of a bluish-green color, exhibit a range of color gradations including blue, green, yellow, gray and white (Figure 1 and Figure S1 in Supporting Information S1). Blue particle aggregates generally have an elongated or ovoid shape and less commonly irregular shapes or sharp edges. SEM images of blue particle interiors show that they are nearly exclusively composed of sub-micron carbonate grains with the remains of few other biogenic particles such as diatoms or coccoliths embedded within the carbonate matrix (Figure 1).

The morphology of the trap particles can be compared with the morphology of carbonates freshly excreted from fasting fish under laboratory conditions (Figure 3). These fish carbonates showed a similar morphology to the blue particles, being commonly greenish-blue or white (occasionally yellow) and generally characterized by irregular shapes and slight elongation. SEM images showed that the fish carbonates comprised of sub-micron elliptical particles, although there was a range in particle morphologies.

3.3. Mineralogy

We performed Rietveld refinement on the XRD data, which allows for the quantification of the individual mineral phases that comprise samples and yields various phase-specific chemical and crystallographic parameters (Bish & Howard, 1988). An example of Rietveld refinement results is shown in Figure S3 in Supporting Information S1. The relative mineral abundances derived from Rietveld refinement for the blue particles and bulk OFP samples are archived in Hashim et al. (2025d). Calcite is often classified into low-Mg calcite (LMC) where the $MgCO_3 \leq 4$ mol%, high-Mg calcite (HMC) where MgCO is between 4 and 20 mol%, and very high-Mg calcite (VHMC) where $MgCO_3$ >20 mol% (Hashim & Kaczmarek, 2021; Hashim et al., 2024). The blue particles are predominately comprised of VHMC (87% relative mineral abundance, on average) with the remainder being aragonite, except one sample that also contains HMC (Figure S5 in Supporting Information S1).

Comparison of raw data and phases calculated via Rietveld refinement for blue particles, fish carbonates, a bulk sediment trap sample from 500 m (OFP 1/85 500 < 37 μm), bryozoan, and coccolith calcite, reveal that the blue particles are characterized by substantially broad peaks with higher 2θ values (Figure 7a). Two calcite peaks can be distinguished in the blue particle XRD data, whose positions reveal that the mineralogy is VHMC, and their widths indicate small crystallite size and/or highly strained material. While all blue particle data are characterized by broad peaks that are generally shifted toward higher 2θ values, there is a large variability across samples in terms of peak widths and positions (Figure 8). Fish carbonates have similar characteristics to the blue particles in terms of peak widths but many of the peaks are shifted toward lower 2θ values and only one overlaps with those of the blue particles (Figure 7b). In contrast, coccolith and bryozoan XRD data exhibit sharp and single peaks and while they overlap with some of the fish carbonate peak positions, they are distinctively narrower (Figure 7c). OFP samples (<125 μm size fraction) are primarily comprised of two calcite phases (Figure 8), in addition to other minor phases (Figures S3 and S5 in Supporting Information S1).

We analyzed the small size fraction (<125 μm) of bulk OFP samples in order to determine whether the blue particles get disaggregated as they sink and are captured as fine particles. The analyzed bulk OFP samples do not

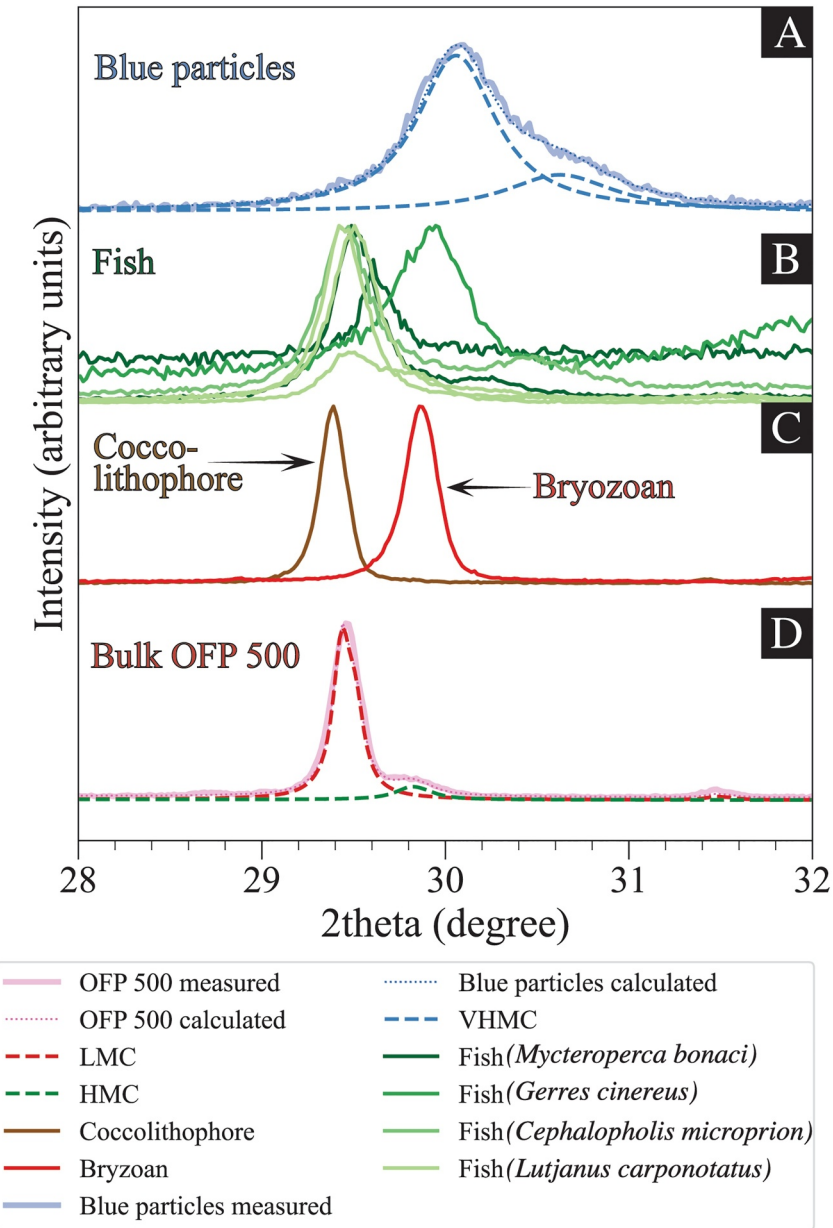

Figure 7. XRD scans of various samples cropped between 28 and 32° 2θ (full scans are shown in Figure S2 in Supporting Information S1). (a) Measured scan of a blue particle sample (4/19-4) along with the calculated profile using two distinct calcite structures fitted using Rietveld refinement (Rwp = 11.2). The blue particle calcite is referred to as very high Mg calcite (VHMC). (b) Measured scans of fish carbonates from fish collected from The Bahamas and Lizard Island, Australia. (c) Measured scans of coccolithophores from a lab culture and bryozoan isolated from Sargassum from Bermuda. (d) Measured scan of a bulk sample (OFP 1/85 500 < 37 μm) from the Oceanic Flux Program (OFP) from 500 m collected in January 1985 along with the calculated profile via Rietveld refinement (Rwp = 5.1) using two calcite structures (LMC and HMC).

contain phases with a mineralogical composition similar to the blue particles. The major calcite phase in the bulk OFP samples typically has a relatively narrow peak and shifted to lower 2θ angles indicating low Mg content (Figure 7d). In contrast, the minor calcite phase has a broader peak and higher 2θ angle hence higher Mg content (Figure 7a). The prominent calcite peaks of these two phases resemble those of coccolithophore and bryozoan samples in terms of 2θ position and peak width (Figure 7d).

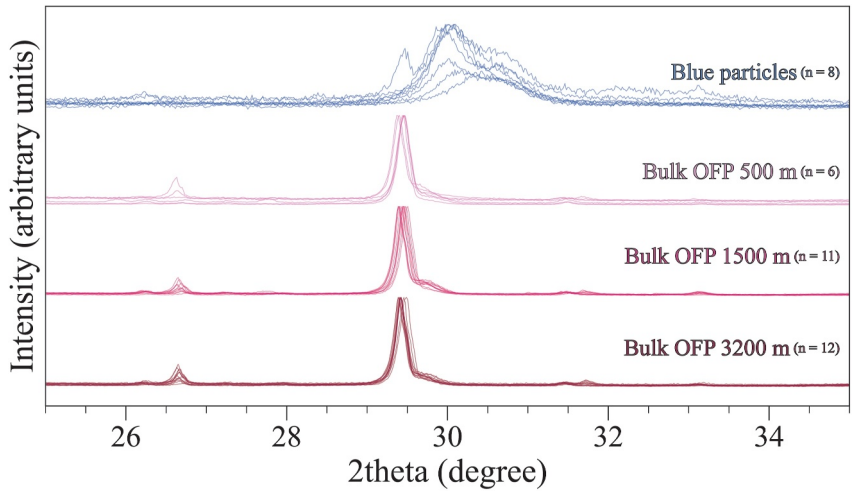

Figure 8. Raw XRD scans were truncated between 25 and 35° for blue particle samples and bulk OFP samples from 500, 1,500, and 3,200 m sediment traps. Full scans are shown in Figure S2 in Supporting Information S1.

One of the parameters that can be calculated via Rietveld refinement is the amount of structural Mg in the calcite crystal lattice using the refined unit cell parameters (e.g., Hashim et al., 2022). The Mg content of the blue particle calcite is highly variable and ranges between 17 and 46 mol% with a weighted mean of 32 ± 10 mol% (SD) (Figure 9). The weighted mean was calculated by taking into account the relative abundances of phases in each sample. This was done because most samples were comprised of multiple phases (including multiple calcite phases). The calculations involved multiplying the $MgCO_3$ of each phase by its abundance, summing the products and dividing the sum by the sum of the phase abundances (typically ~ 100%). For example, if a sample contains 90% of a calcite phase with 30 mol% $MgCO_3$, 5% of a second calcite phase with 7 mol% $MgCO_3$, and 5% aragonite (0 mol% $MgCO_3$), the $MgCO_3$ weighed mean is 27 mol%.

Freshly collected fish carbonate $MgCO_3$ (from fish under laboratory conditions) is even more variable than the sediment trap blue particles ranging between 0.21 and 38 mol% (Figure 9) with an interquartile range of 28.5 mol% (Table S2 in Supporting Information S1). Importantly, the only end member with an Mg content as

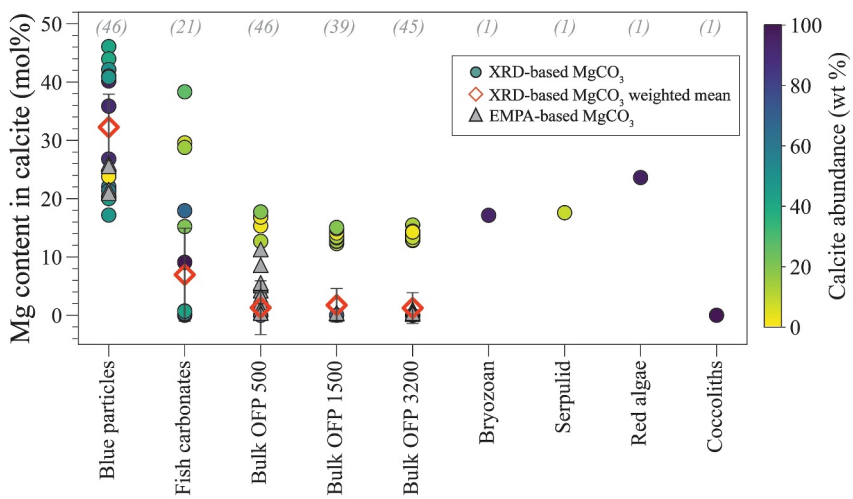

Figure 9. The Mg content of calcite as mol% $MgCO_3$ in various samples derived from XRD and EMPA. The XRD-derived data is color-coded by the abundance of the calcite phase in the sample. Most samples contain more than one phase, and each phase is represented as a circle. Also plotted is the weighted mean, which was calculated using the Mg content and the relative abundance of each phase in the sample. The error bars represent the margin of error around the mean derived for a 95% confidence interval. EMPA refers to the electron microprobe data. The gray number in parentheses denotes the number of datapoints for each sample type.

high as the blue particles is fish carbonates (Figure 9). (The fish carbonate samples also contained quartz from contaminating fragments from the quartz airstones used for tank aeration.) While some of the fish carbonate $MgCO_3$ overlap with those of the blue particles, it is observed that the fish carbonates of the analyzed samples are comprised of calcite with lower Mg content. Indeed, the *p* value suggests that the difference in the Mg content of the blue particles and fish carbonate is statistically significant (Table S2 in Supporting Information S1).

The bulk OFP samples are dominated by LMC, followed by HMC followed by minor amounts of aragonite, quartz, kaolinite, and halite (Figure S5 in Supporting Information S1). Calcites in the bulk OFP sample have <18 mol% $MgCO_3$ (Figure 9) as determined by the refined unit-cell parameters. Bryozoan and serpulid carbonates are comprised of HMC and their Mg contents match the upper end of the OFP samples, but are lower than, and do not overlap with the Mg content of the blue particles (Figure 9). The red algae carbonate has a higher Mg content than bryozoan and serpulid that overlaps with the blue particles (Figure 9). The Mg content of the coccoliths is ∼0, which matches, within the measurement uncertainty, the lower end of the bulk OFP samples from 500, 1,500, and 3,200 m (Figure 9). The XRD-derived Mg content of blue particle calcite is statistically significant when compared with fish carbonates, coccolithophores, and bulk OFP (*p* values < 0.05) and statistically insignificant when compared with red algae, bryozoan, and serpulid (*p* values > 0.05; Table S2 in Supporting Information S1).

The Mg content derived from EMPA data is in agreement with the XRD-derived data (Figure 9) with the exception of OFP samples from the deeper traps at 1,500 and 3,200 m, in which no HMC was found via EMPA. The elemental maps collected for a blue particle from sample OFP 4/19-3 500 reveal distinct zonation in the Mg and Ca (Figure 4). Specifically, the core of the particle is Mg rich and contains less Ca, whereas the rim is Mg poor and contains more Ca (Figures 4b and 4c). Furthermore, the particle is characterized by a thin outer zone of higher phosphorous content compared to the particle core (Figure 4d). It should be noted that we collected an EMPA map for only one blue particle where we observed zonation. It is still to be determined whether this is a feature that characterizes other blue particles and fish carbonates in general. Examples of SEM photos with analyzed spots are shown in Figure S6 in Supporting Information S1.

3.4. Carbonate Isotopic Composition

The inorganic carbon content of the blue particles has a $\delta^{13}C_{Inorg}$ ranging between −3.8 and −1.3‰ (average −2.4 ± 0.7‰) and $\delta^{18}O_{Inorg}$ between 1.4 and 3.5‰ (average 2.6 ± 0.6‰) (Table 2 and Figure 5). The bulk OFP samples (<125 μm fraction) $\delta^{13}C_{Inorg}$ ranges from −0.26 to 1.23‰ (with average 0.4 ± 0.6‰) and $\delta^{18}O_{Inorg}$ ranges from −0.03 to 1.18 (with average 1.12 ± 0.4‰), with overlapping ranges across samples from sediment traps at 500, 1,500, and 3,200 m (Table 2, Figure 5, Hashim et al., 2025c). The isotopic composition of pteropods and foraminifera species picked from the OFP traps, both of which are large-sized carbonate producers contributing to the carbonate flux, shows a relatively wide range, closely aligning with the OFP composition. Specifically, pteropods (*C. columnella*, *C. virgula conica*, *C. acicula*, *C. pyramidata*, *D. quadridentate*, *S. subula*, *H. inflatus*) exhibit $\delta^{13}C_{Inorg}$ values ranging from −1.11 to 2.28‰, with an average ± 1 s.d. of 0.67 ± 0.5‰, and $\delta^{18}O_{Inorg}$ values ranging from −0.65 to 1.90‰, with an average of −0.95 ± 0.49‰. Foraminifera (*P. obliquiloculata*, *G. truncotulinoidee*, *G. bulloides*, *G. Inflata*, *N. dutertrei*, *G. Ruber*, *G. conglobotus*, *G. aequilateralis*, *O. universa*, *G. hirsute*) exhibit $\delta^{13}C_{Inorg}$ values ranging from −2.40 to 1.63‰, with an average of 0.076 ± 0.67‰, and $\delta^{18}O_{Inorg}$ values ranging from −1.95 to 1.17‰, with an average of −0.57 ± 0.66‰. Neritic shallow water detrital carbonate sediments from the Bermuda Pedestal, collected in the OFP traps following hurricane-induced sediment transport events (Pedrosa-Pamies et al., 2025), are also distinct from the blue particles with $\delta^{13}C_{Inorg}$ value of 1.77‰ for the 500 m sample and 1.49‰ for the 1,500 m sample and $\delta^{18}O_{Inorg}$ value of −0.44 ‰ for the 500 m sample and −0.59‰ for the 1,500 m sample (Table 2 and Figure 5).

Epibiont carbonates on Sargassum are also distinctive from the blue particles. The $\delta^{13}C_{Inorg}$ of bryozoan (*M. tuberculata*) ranges from −4 to −1.7 with an average of −2.34 ± 0.7‰, overlapping with the $\delta^{13}C_{Inorg}$ of the blue particles, but the $\delta^{18}O_{Inorg}$ are more depleted ranging from −1.16 to −0.43 with an average of −0.73 ± 0.3‰. The serpulid worm tubes (*Neodexiospira*) have an average $\delta^{13}C_{Inorg}$ of 1.07 ± 0.1‰ and $\delta^{18}O_{Inorg}$ of −0.4‰ ± 0.02. Finally, subtropical benthic red alga (*Neogoniolithon*) is also depleted in $\delta^{13}C_{Inorg}$ and $\delta^{18}O_{Inorg}$ of −3.7 ± 0.01 and −5.4‰ ± 0.01, respectively, relative to the blue particles.

The isotopic composition of coccoliths is sourced from cultured coccolithophore for the following five species: *Gephyrocapsa oceanica, E. huxleyi*, *Coccolithus braarudii*, *Thoracosphaera heimii*, and *Calcidiscus leptoporus*

(Hermoso et al., 2014). The media in which the coccolithophores were cultured has a $\delta^{13}C_{DIC}$ of −0.02 and $\delta^{18}O_{H2O}$ of −0.69‰ which fall within the isotopic ranges of seawater at the OFP site (see below). The $\delta^{13}C_{Inorg}$ of the coccoliths ranges from −5.7 to 2 with an average of −1.1 ± 2.9‰ and $\delta^{18}O_{Inorg}$ ranges between −1.1 and 2.9 with an average of 0.6 ± 1.5‰.

Fish carbonates (*Sphyraena barracuda*, *Mycteroperca bonaci*, *A. vulpes*, *S. testudineus*, *Cephalopholis cruentata*, *L. apodus*, *Gerres cinereus*, *Ocyurus chrysurus*, *Lutjanus carponotatus*) are characterized by $\delta^{13}C_{Inorg}$ ranging from −6.7 to 2.7 with an average of −1.8 ± 1.9 ‰ and $\delta^{18}O_{Inorg}$ ranging from −1.4 to 2.1 with an average of 0.9 ± 0.8‰. The isotopic composition of fish carbonate is generally similar to that of the blue particles (Table 2). Both have distinctively negative $\delta^{13}C_{Inorg}$ and positive $\delta^{18}O_{Inorg}$, with the notable observation that the particles have higher $\delta^{18}O$ and narrower range of $\delta^{13}C$ compared to the fish carbonates. Fish carbonates from the sardine fed fishes are generally more depleted in $\delta^{13}C$ compared to carbonates from fishes fed a mixed diet (Figure 5). The stable isotope ratio of organic carbon was not measured in either the mixed diet or the sardine diet. However, existing data indicate that the mixed diets of our fish species from The Bahamas are mainly comprised of other fishes and crustaceans, which are characterized by $\delta^{13}C$ values of −15 to −14‰ based on previous studies (Kieckbusch et al., 2004; Lamb et al., 2012). In contrast, the sardine diet is expected to have $\delta^{13}C$ values of −20 to −18‰ based on the observation that zooplankton (the main dietary component of *S. aurita*) has a $\delta^{13}C$ of −21.9 to −20.5‰ in the Gulf of Mexico (Thayer et al., 1983) and that carbon isotope fractionation in sardines results in a 2‰ enrichment over their dietary intake (Bode et al., 2004). The differences in $\delta^{13}C$ between the blue particles and all other categories are statistically significant except fish carbonates, red algae, and bryozoan based on a threshold of 0.05 (Table S2 in Supporting Information S1). Differences in $\delta^{18}O$ between the blue particles and all other sample categories are statistically insignificant (p values << 0.05; Table S2 in Supporting Information S1).

Measured $\delta^{13}C$ seawater DIC at the nearby BATS site ranges between 0.31 and 0.88 ‰ in the upper 500 m of the water column (Table S1 in Supporting Information S1). Given that seawater $\delta^{13}C$ has been decreasing due to the release of ^{13}C-depleted anthropogenic CO_2 into the atmosphere and its subsequent uptake by the ocean (Keeling et al., 2004), we estimate seawater $\delta^{13}C$ at BATS between 1990 and 2020 (the interval during which the blue particles are observed) to range between −0.7 and 2.47 ‰ taking into consideration a 0.4 ‰ seasonal variability (Brooks, 2020). This demonstrates that the blue particles are depleted in $\delta^{13}C$ compared with ambient seawater (Figure 5).

To estimate the formation temperature of the blue particles, we calculated the $\delta^{18}O_{calcite}$ using seawater $\delta^{18}O$ at BATS and various oxygen fractionation factors (α) in calcite from Kim and O'Neil (1997), Watkins et al. (2013), and Mavromatis et al. (2012). Seawater $\delta^{18}O$ ranges from −29.64 to −28.52 ‰ with an average of −28.92 ± 0.07 ‰ on the VPDB scale (Figure 6b). The calculated $\delta^{18}O_{calcite}$ ranges from −1.16 to 0.73 ‰ with an average of 0.34 ± 0.45 ‰ using the α of Kim and O'Neil (1997) and from 0.55 to 2.35 with an average of 1.98 ± 0.43 using α of Watkins et al. (2013) (Figure 6c). Propagating the observed variability in temperature (Figure 6a) and $\delta^{18}O_{sw}$ (Figure 6b) into the calculated $\delta^{18}O_{calcite}$ reveals that the $\delta^{18}O_{calcite}$ can be as low as −4.0‰ and as high as 3.46‰ in the upper 100 m of the water column (Figure 6c). The upper portion of this range encompasses the measured blue particle $\delta^{18}O$ values which range from 1.44 to 3.46‰ with an average of 2.58 ± 0.45‰ (Figure 6c). Further, we calculated α using the data of Mavromatis et al. (2012) who determined α as a function of mol% $MgCO_3$ and temperature assuming an $MgCO_3$ in calcite of 1, 10, 20, and 32 mol%. The 1 and 10 mol% $MgCO_3$ yielded $\delta^{18}O_{calcite}$ that are similar but slightly more enriched than that calculated using the fractionation factors of Kim and O'Neil (1997) and Watkins et al. (2013), respectively (Figure 6c). The 20 and 32 mol% generally give more enriched $\delta^{18}O_{calcite}$ that the range of the blue particles (Figure 6c).

4. Discussion

4.1. Origin of the Blue Particles

The blue particles found in the Oceanic Flux Program (OFP) sediment traps have distinctive morphological, mineralogical, elemental, and isotopic characteristics compared with other biogenic pelagic carbonates produced by coccolithophores, foraminifera, and pteropods. The unusually high and variable blue particle Mg content (17–46 with an average of 32 ± 10 mol% $MgCO_3$) and isotopic compositions are atypical of common marine calcifiers and much higher than the carbonate in the fine (<125 μm) size fraction of OFP samples, which makes up the bulk of the carbonate flux (Table 2 and Figures 5 and 9). The distinctive mineralogical and isotopic characteristics indicate that the blue particles have a unique origin compared with typical pelagic carbonate sources in the particle

flux. While bryozoans and serpulid worms, both epiphytes on floating *Sargassum* weed, are potential sources of HMC, our analysis indicates that bryozoans and serpulids produce HMC with lower $MgCO_3$ (17 and 18 mol%, respectively, Figure 8). Neritic sediments advected from the Bermuda Pedestal to the OFP site during hurricanes Fabian and Igor (Pedrosa-Pamies et al., 2025) also have a very different isotopic composition than the blue particles (Figure 5), indicating that the blue particles are unlikely to be of shallow water detrital carbonate origin.

The blue particles in the OFP traps have characteristics much more similar to carbonates produced by fish, suggesting that they are fish-derived. First, the blue particle aggregates resemble fish carbonate aggregates in color, morphology, size, and texture, and the individual submicron grains are morphologically similar (Figure 1; Figures S1 and S3 in Supporting Information S1). The distinctive greenish blue color of the OFP trap particles, in particular, is characteristic of many fish carbonates and is suggested to be caused by bile secreted from the gall bladder into the intestine (Cornelius, 1991). Furthermore, the ellipsoidal morphology of the submicron-sized grains in the blue particles is similar to that of fish, and has been proposed to reflect precipitation from highly supersaturated solution intestinal fluid of marine teleosts where pH ranges between 8.3–9.2 and TA between 30–100 mM (Grosell, 2019; Wilson et al., 2002).

The unusually high Mg content (up to 46 mol% $MgCO_3$) of the blue particles (Table 2; Figure 9) is generally similar to fish carbonates, particularly for *Cephalopholis microprion* (freckled hind, sampled from Lizard Island, Great Barrier Reef, Australia) whose calcite has the highest Mg content of all the analyzed fish carbonate samples (Figure 9). These similarities are further supported by published fish carbonate XRD data from 8 sub-tropical reef fish species (Perry et al., 2011; Salter et al., 2019), wherein the main calcite peaks (d104) are similarly broad and reportedly indicate that primary components are HMC and VHMC containing 13–30 mol% $MgCO_3$. The generally higher Mg contents reported in those studies compared to the fish carbonates analyzed here may be due to samples being from different fish species, as Mg content is known to vary among species (Salter et al., 2018).

4.2. Formation Mechanism of the Blue Particles

The mineralogical composition of the blue particles necessitates precipitation from chemically modified seawater. The typical Mg/Ca in abiotic calcite precipitation from seawater is ∼12 mol% assuming a water temperature of 22°C and 6 mol% assuming a temperature of 15°C (Hashim & Kaczmarek, 2022; Morse et al., 2007). Accordingly, if the blue particles formed abiotically from average seawater, they would contain a much lower Mg content. As Mg incorporation into calcite increases its solubility for calcites with >4 mol% Mg (Morse et al., 2006), a highly supersaturated solution is needed to precipitate calcite with the mineralogical composition of the blue particles, implying that the blue particles were precipitated in a closed or semi-closed system. Precipitation from a highly supersaturated solution is further supported by the mineralogy and texture of the blue particles (Figure 1), which are comprised of small, highly strained crystallites as evidenced by the breadth of the XRD peaks (Figure 8). While the mineralogy of the blue particles is high-Mg calcite, it is possible that the original phase was amorphous calcium magnesium carbonate (ACMC). The morphology and texture of the blue particles hold close resemblances to those of ACMC (Blue et al., 2017) and some fish carbonates have also been found to be comprised of ACMC (Perry et al., 2011). This suggests that the blue particles may have experienced mineralogical transformation in the gut and/or after their excretion.

Fish intestines represent a suitable semi-closed environment where ingested seawater is altered by water absorption and intestinal bicarbonate secretion, increasing Ω with respect to carbonate minerals (Wilson et al., 2002). The distinct chemical zonation indicated by the EMPA analysis (Figure 4) implies a chemically evolving solution during precipitation, consistent with a closed system environment. Precipitation in a chemically modified closed system whose composition evolves with time could also explain their isotopic enrichment as well as mineralogy (Figures 5 and 9). Such elemental zonation also implies that the blue particles may have experienced partial dissolution following their precipitation.

A weak correlation between the Mg content and $\delta^{13}C$ of the blue particles (Figure 10) hints to the idea that as fish modify their intestinal fluids and mix respired CO_2, they create a highly supersaturated, ^{13}C-depleted solution. As precipitation proceeds, Ω decreases and the $\delta^{13}C$ evolves toward less depleted values, resulting in the observed trend of decreasing Mg content and increasing $\delta^{13}C$. Closed system precipitation could also explain the apparent insensitivity of the blue particle $\delta^{13}C$ to external environmental variables such as temperature, salinity, and Ω (Figures S8d–S8f in Supporting Information S1).

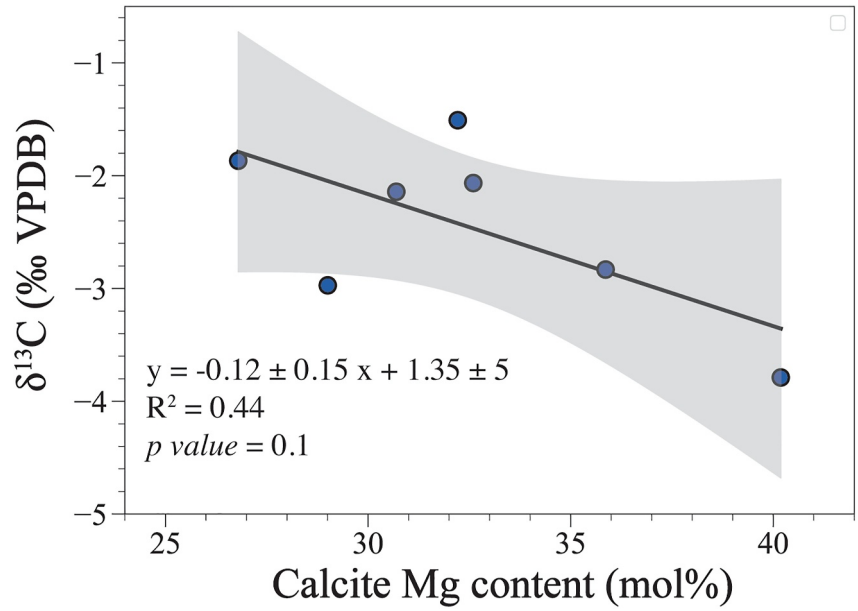

Figure 10. Cross plot between Mg content in blue particle calcite (mol%) calculated as the weighted mean against their ^{13}C values with 95% confidence interval. Also shown are the regression equation, *r* squared, and the *p* value.

Several processes can impact the isotopic composition of biogenic carbonates, including metabolic effects that modify the isotopic composition of DIC (McConnaughey, 1989a; McConnaughey et al., 1997), kinetic effects that discriminate against heavy isotopes (McConnaughey, 1989b), and Rayleigh fractionation whereby the fluid isotopic composition evolves as a result of precipitation from a closed system (Chen et al., 2018). Assuming that the blue particles are produced by fish, respired carbon, which is typically depleted in $\delta^{13}C$, could modify the $\delta^{13}C$ of the DIC pool from which the blue particles precipitate, leading to the observed depleted $\delta^{13}C$ of the blue particles (Figure 5). Diet would then play a role in shaping the blue particle isotopic composition, as the source of respired CO_2 in fish is dietary carbon (Oehlert, Garza, et al., 2024). Indeed, carbonates excreted from fish fed a sardine diet, which is ~3‰ lower in $\delta^{13}C_{org}$ compared with a mixed diet, are also depleted in $\delta^{13}C_{Inorg}$ compared with fish fed a mixed diet (Figure 5). If produced by fish, the wide variability in $\delta^{13}C_{Inorg}$ of the blue particles suggests that they were produced by multiple fish species and/or under different dietary conditions. Kinetics is also known to lead to depleted isotopic compositions in carbonates (Watkins et al., 2014). Given that fish intestinal fluids are highly supersaturated (Wilson et al., 2002), fish carbonates likely precipitate quickly, which could explain their depleted $\delta^{13}C$ (Figure 5).

The $\delta^{18}O$ of the blue particles ($\delta^{18}O_{bp}$) could also be influenced by the kinetics in addition to the formation temperature and $\delta^{18}O_{sw}$. We used seawater temperature (Figure 6a), $\delta^{18}O_{sw}$ calculated from salinity (Figure 6b), and experimentally derived oxygen isotope fractionation factors (Kim & O'Neil, 1997; Mavromatis et al., 2012; Watkins et al., 2013) to calculate the equilibrium $\delta^{18}O_{calcite}$ precipitating from seawater in the upper 500 m (Figure 6c). The $\delta^{18}O_{bp}$ values are generally more enriched than the calculated $\delta^{18}O_{calcite}$ but their ranges overlap especially when considering the seasonal variability in temperature and $\delta^{18}O_{sw}$, which leads to a wide range of possible $\delta^{18}O_{calcite}$ particularly in the upper ~100 m (Figure 6c). This comparison between the measured $\delta^{18}O_{bp}$ and the calculated $\delta^{18}O_{calcite}$ suggests that the blue particles could have formed anywhere in the upper 500 m of the water column (Figure 6c). Furthermore, $\delta^{18}O_{bp}$ is inversely correlated, albeit weakly, with seawater temperature in the mixed layer (Figure S8g in Supporting Information S1), indicating that the seasonal temperature fluctuation in the upper ocean has an impact on the $\delta^{18}O_{bp}$. An alternative explanation to this relationship is that some blue particles have formed at shallow depths from warmer water, leading to lower $\delta^{18}O_{bp}$ while others formed deeper from colder water, leading to higher $\delta^{18}O_{bp}$. Furthermore, the higher $\delta^{18}O_{bp}$ values compared with those of the fish carbonates (Figure 5) could imply that the blue particles have formed at lower temperatures than the analyzed fish carbonates. Such an interpretation is plausible because seawater temperature at BATS ranges from ~21 to 28°C in the upper 100 m and declines to ~16°C at 500 m (Figure S7 in Supporting Information S1),

whereas the analyzed fish carbonates were obtained from fish collected or maintained at generally higher temperatures ranging from 24 to 31°C (Hashim et al., 2025c).

Notably, the $\delta^{18}O_{bp}$ values only partially overlap with the equilibrium $\delta^{18}O_{calcite}$ and only with the curve calculated using the fractionation factor of Watkins et al. (2013) (Figure 6c). This fractionation factor is considerably higher than most other studies (e.g., Dietzel et al., 2009; Jiménez-López et al., 2004; Kim & O'Neil, 1997; Tarutani et al., 1969; Watson, 2004), and is thought to represent the true equilibrium fractionation factor for oxygen isotopes in calcite (Watkins et al., 2014). However, there is no evidence that the blue particles formed in isotopic equilibrium with the precipitating fluid. The partial overlap of $\delta^{18}O_{bp}$ with the calculated equilibrium $\delta^{18}O_{calcite}$ possibly stems from kinetics and mineralogical effects acting in opposite directions, thus leading to $\delta^{18}O_{bp}$ values that are seemingly in equilibrium with seawater, as discussed below.

Kinetics typically lower the fractionation factor by up to 2 ‰ from the equilibrium value (Dietzel et al., 2009; Gabitov et al., 2012; Watkins et al., 2013), implying that the $\delta^{18}O_{bp}$ should be more depleted than the equilibrium calcite but instead they are more enriched (Figure 6c). The fact that the blue particles are comprised of high-Mg calcite can lead to enrichment in their $\delta^{18}O_{bp}$ (Mavromatis et al., 2012). Accordingly, $\delta^{18}O_{bp}$ values being lower than the predicted composition for calcite with their average $MgCO_3$ of 32 mol% (Figure 6c) could be related to kinetics that counteracted the effect of mineralogy. It should be noted that the effect of calcite Mg content on oxygen fractionation is not very well constrained (Jiménez-López et al., 2004; Mavromatis et al., 2012); thus, the exact contribution of kinetics versus mineralogy in setting the blue particle isotopes is currently unknown. Furthermore, as mentioned earlier, the original phase of the blue particles could have been ACMC, which has been shown to exhibit higher oxygen isotope fractionation compared to the equilibrium value (Dietzel et al., 2020). The enriched $\delta^{18}O_{bp}$ could be related to the formation pathway via ACMC that subsequently recrystallizes to high Mg calcite. More detailed laboratory work on carbonate secretion by fish that is capable of capturing the initial phases that form, and their subsequent transformation will provide a more direct test to the proposed hypothesis.

Isotopic enrichment could also be introduced via Rayleigh distillation, that is, the progressive change in the isotopic composition of fluids as a result of isotopic fractionation and precipitation in a closed system. If the blue particles form in fish intestines, as do other fish carbonates, their isotopic composition will be affected by the composition of the intestinal fluids. Marine fish significantly alter their intestinal fluids as part of their osmoregulatory strategy by secreting HCO_3^- and absorbing water (Grosell, 2019; Grosell & Oehlert, 2023; Wilson et al., 2002). These processes involve the exchange of numerous ions across the intestinal wall and could lead to isotope fractionation. If the lighter ^{16}O is preferentially adsorbing during osmosis, the intestinal fluids from which $CaCO_3$ precipitates will become progressively isotopically enriched, leading to a progressive increase in $\delta^{18}O$ of precipitated carbonates. While it is currently unknown whether osmosis in general leads to oxygen isotope fractionation, such an effect has been demonstrated for lithium where membrane diffusion of the heavier isotope (^7Li) is slightly slower than its lighter counterpart (^6Li) (Whitworth et al., 1994). Future work is needed to explore the isotope fractionation of carbon and oxygen during osmoregulation in fish and its impact on the isotopic composition of the precipitated carbonates.

4.3. Abundance, Seasonality, and Fate of the Blue Particles

Although the OFP traps continuously sample the mesopelagic particle flux in the Sargasso Sea, blue particles have only been encountered in 14 samples, or <1% of the samples collected since 1992 (Table 1, Figure 2). Spatial heterogeneity in fish biomass (Dimarchopoulou et al., 2024; García-Charton et al., 2004) cannot be invoked to explain their rarity, as the "statistical funnel" of flux collected by the 500 m trap is mesoscale in area, even for particles sinking at a rate of 200 m/d (Siegel & Armstrong, 2002). An alternative explanation for the sporadic nature of the blue particles is that due to their fragility, blue particle aggregates will rapidly disintegrate post defecation with the submicron HMC particles being subject to rapid dissolution due to the high solubility of HMC (Dean et al., 2024; Subhas et al., 2022; White et al., 2018). While we did not detect mineral phases that resemble the blue particles in our XRD analyses of the <125 μm size fraction of OFP samples (Figure 7), a more comprehensive mineralogical analysis is needed to ascertain if mineral phases resembling that of the blue particles occur in trace quantities in the very fine size fraction of the flux material.

The blue particles in the OFP traps were found exclusively between November and May, with >50% of the occurrences in December and January (Table 1, Figure 2b). This seasonality coincides with the onset of the

seasonal peak in surface ocean productivity (Lomas et al., 2013) and in the magnitude and lability of the particle flux (Conte et al., 2001, 2025), and thus could be a reflection of greater mesopelagic fish activity around the 500 m trap. It is possible that the blue particles in the traps are a fortuitous consequence of fish congregating around sediment traps to feed, as the 500 m trap often contains fish debris (Conte et al., 2025). Although the greater occurrence of blue particles during the December–January time period cannot be directly correlated with a higher presence of fish debris in the trap samples, a better understanding of fish seasonal variability in the region and fish behavior around traps could help inform this possibility as to the origin(s) of the blue particles.

It is worth noting that studies of fish-produced carbonate thus far have focused on fish species from coastal, shallow-water and reef settings (Folkerts et al., 2024; Ghilardi et al., 2023; Oehlert, Garza, et al., 2024; Salter et al., 2012, 2014, 2017), and that nothing is known about carbonates excreted by open ocean pelagic fish. While the blue particles and carbonates excreted by tropical, shallow marine fish analyzed here are generally similar, there are notable differences between them. For example, the blue particle aggregates are generally smaller (Figures 1 and 3), characterized by higher Mg contents (Figure 9), and enriched in $\delta^{18}O$ (Figure 5). If the blue particles are in fact fish-derived, the differences noted here suggest unique styles of production, dissolution, and export of fish-produced carbonates in the open ocean that arise from differences in pelagic fish physiology, diet and habitat.

4.4. Implications and Conclusions

This study provides the first evidence of fish carbonate production in the open ocean, supporting the idea that carbonate production by fish is a global phenomenon (Walsh et al., 1991; Wilson et al., 2009), and that fish contribute to the production, export, and dissolution of $CaCO_3$ in the open ocean. We show that the mineralogy, elemental composition, morphology, size, and texture of the blue particles, which we hypothesize were produced by open ocean fish, are generally similar to fish carbonates from shallow marine environments (Figures 1, 3, and 4), suggesting that these characteristics are likely the result of the mechanism by which teleost fish precipitate carbonate in their intestines. That said, we note that the blue particle mineralogical and isotopic compositions are highly variable and generally have higher Mg contents and $\delta^{18}O$ and lower $\delta^{13}C$ than the fish carbonates collected in laboratory settings (Figures 5 and 9). These differences could reflect the experimental conditions to which fish were subjected, chief of these being diet as fish in laboratory settings were not provided with food during carbonate sampling. As such, investigating fish produced carbonates in nature complements laboratory studies in significant ways.

The distinctive mineralogy and isotopic composition of the blue particles and fish carbonates compared to major pelagic carbonate producers (Figure 5) speaks to the uniqueness of fish carbonates and the unusual mechanism by which they form. We propose that the blue particles form in fish intestines in a closed system from a highly supersaturated, Mg-rich seawater derived fluid capable of precipitating calcite with high Mg content and an isotopic composition in disequilibrium with ambient seawater. This hypothesis implies that the isotopic and elemental composition of fish carbonates is impacted by a combination of metabolic effects, kinetics, mineralogical transformations, and fractional distillation.

Fish carbonates are highly prone to rapid dissolution and will contribute to excess ocean alkalinity (Wilson et al., 2009). Present uncertainties about the solubility and dissolution rates of pelagic fish carbonates have implications for the depth of the fish carbonate saturation horizon (Figure S4 in Supporting Information S1) and, as such, the role of fish carbonate production in the ocean carbon cycle. Further study is needed to elucidate the roles of fish in the oceanic carbon cycle in general, and alkalinity excess and carbon export in particular, both of which are currently poorly constrained.

Data Availability Statement

All data used in this study are archived in the BCO-DMO repository. This includes a compilation of OFP samples that contain blue particles (Hashim et al., 2025a), metadata on the end members that are compared to the blue particles (Hashim et al., 2025b), the carbonate $\delta^{13}C$ and $\delta^{18}O$ for various sample types measured in the study and compiled from the literature (Hashim et al., 2025c), and XRD results and associated XRD raw data (Hashim et al., 2025d).

Acknowledgments
The OFP time-series is supported by the US National Science Foundation Chemical Oceanography Program (NSF OCE), most recently by Grants 2122619, 2414704, and 2421112. MSH acknowledges financial support from the WHOI Postdoctoral Scholar Program and NSF OCE Postdoctoral Fellowship (award #2205984). MAS and RWW acknowledge financial support from a UK NERC BIO-Carbon Grant (NE/X008649/1). Fish carbonate samples were collected by MAS, RWW, and CTP under NERC Grant NE/K003143/1. AVS acknowledges support from NSF OCE (awards #1923998 and 2123055). *Sargassum* samples were collected on U.S. GO-SHIP line A22 with the support of NSF and NOAA as well as on a BATS cruise aboard the R/V *Atlantic Explorer*. We greatly appreciate the efforts of all who participated in the collection, processing, and preservation of the samples. Dennis McGillicuddy gratefully acknowledges the support provided by WHOI and the Isham Family Charitable Fund. We would like to thank Jeff Turner, Eve Arnold, Dorinda Ostermann, and Steven Manganini for their assistance with initial analyses of the blue particles which inspired this study, and Steve Clemens, Chloe Dean, Jim Eckert, Dennis McGillicuddy, Charlie Settens for helping with various analyses, and the reviewers for their feedback which improved the manuscript.

References

Adkins, J. F., Naviaux, J. D., Subhas, A. V., Dong, S., & Berelson, W. M. (2021). The dissolution rate of $CaCO_3$ in the ocean. *Annual Review of Marine Science*, *13*(1), 57–80. https://doi.org/10.1146/annurev-marine-041720-092514

Babila, T. L., Rosenthal, Y., & Conte, M. H. (2014). Evaluation of the biogeochemical controls on B/Ca of *Globigerinoides ruber* white from the oceanic flux program, Bermuda. *Earth and Planetary Science Letters*, *404*, 67–76. https://doi.org/10.1016/j.epsl.2014.05.053

Berelson, W. M., Balch, W. M., Najjar, R., Feely, R. A., Sabine, C., & Lee, K. (2007). Relating estimates of $CaCO_3$ production, export, and dissolution in the water column to measurements of $CaCO_3$ rain into sediment traps and dissolution on the sea floor: A revised global carbonate budget: A revised global carbonate budget. *Global Biogeochemical Cycles*, *21*(1). https://doi.org/10.1029/2006GB002803

Bevington, P. R., & Robinson, D. K. (2003). Data reduction and error analysis.

Bischoff, W. D., Mackenzie, F. T., & Bishop, F. C. (1987). Stabilities of synthetic magnesian calcites in aqueous solution: Comparison with biogenic materials. *Geochimica et Cosmochimica Acta*, *51*(6), 1413–1423. https://doi.org/10.1016/0016-7037(87)90325-5

Bish, D. L., & Howard, S. A. (1988). Quantitative phase analysis using the Rietveld method. *Journal of Applied Crystallography*, *21*(2), 86–91. https://doi.org/10.1107/s0021889887009415

Black, D. R., Mendenhall, M. H., Brown, C. M., Henins, A., Filliben, J., & Cline, J. P. (2020). Certification of standard reference material 660c for powder diffraction. *Powder Diffraction*, *35*(1), 17–22. https://doi.org/10.1017/s0885715620000068

Blue, C. R., Giuffre, A., Mergelsberg, S., Han, N., De Yoreo, J. J., & Dove, P. M. (2017). Chemical and physical controls on the transformation of amorphous calcium carbonate into crystalline CaCO3 polymorphs. *Geochimica et Cosmochimica Acta*, *196*, 179–196. https://doi.org/10.1016/j.gca.2016.09.004

Bode, A., Alvarez-Ossorio, M. T., Carrera, P., & Lorenzo, J. (2004). Reconstruction of trophic pathways between plankton and the North Iberian sardine (Sardina pilchardus) using stable isotopes. *Scientia Marina*, *68*(1), 165–178. https://doi.org/10.3989/scimar.2004.68n1165

Brand, W. A., Coplen, T. B., Vogl, J., Rosner, M., & Prohaska, T. (2014). Assessment of international reference materials for isotope-ratio analysis (IUPAC technical report). *Pure and Applied Chemistry*, *86*(3), 425–467. https://doi.org/10.1515/pac-2013-1023

Broecker, W., & Clark, E. (2009). Ratio of coccolith CaCO3 to foraminifera CaCO3 in late Holocene deep sea sediments. *Paleoceanography*, *24*(3). https://doi.org/10.1029/2009PA001731

Brooks, M. K. (2020). *Time series of stable isotopes in dissolved inorganic carbon of surface seawater near Bermuda and Hawaii (PhD Thesis)*. University of California.

Chen, S., Gagnon, A. C., & Adkins, J. F. (2018). Carbonic anhydrase, coral calcification and a new model of stable isotope vital effects. *Geochimica et Cosmochimica Acta*, *236*, 179–197. https://doi.org/10.1016/j.gca.2018.02.032

Coelho, A. A. (2018). TOPAS and TOPAS-Academic: An optimization program integrating computer algebra and crystallographic objects written in C++. *Journal of Applied Crystallography*, *51*(1), 210–218. https://doi.org/10.1107/S1600576718000183

Conte, M. H., Pedrosa-Pamies, R., Weber, J. C., & Johnson, R. J. (2025). The climatology of the deep particle flux in the oligotrophic Western North Atlantic gyre, 1978–2022. *Progress in Oceanography*, *234*, 103433. https://doi.org/10.1016/j.pocean.2025.103433

Conte, M. H., Ralph, N., & Ross, E. H. (2001). Seasonal and interannual variability in deep ocean particle fluxes at the Oceanic Flux Program (OFP)/Bermuda Atlantic Time Series (BATS) site in the Western Sargasso Sea near Bermuda. *Deep Sea Research Part II: Topical Studies in Oceanography*, *48*(8–9), 1471–1505. https://doi.org/10.1016/S0967-0645(00)00150-8

Cornelius, C. E. (1991). Bile pigments in fishes: A review. *Veterinary Clinical Pathology*, *20*(4), 106–116. https://doi.org/10.1111/j.1939-165X.1991.tb00868.x

Dean, C., Harvey, E. L., Johnson, M. D., & Subhas, A. V. (2024). Microzooplankton grazing on the coccolithophore *Emiliania huxleyi* and its role in the global calcium carbonate cycle. *Science Advances*, *10*(45), eadr5453. https://doi.org/10.1126/sciadv.adr5453

Deuser, W. G., & Ross, E. H. (1989). Seasonally abundant planktonic foraminifera of the Sargasso Sea; succession, deep-water fluxes, isotopic compositions, and paleoceanographic implications. *Journal of Foraminiferal Research*, *19*(4), 268–293. https://doi.org/10.2113/gsjfr.19.4.268

Deuser, W. G., Ross, E. H., Hemleben, C., & Spindler, M. (1981). Seasonal changes in species composition, numbers, mass, size, and isotopic composition of planktonic foraminifera settling into the deep Sargasso Sea. *Palaeogeography, Palaeoclimatology, Palaeoecology, Oxygen and Carbon Isotopes in Foraminifera*, *33*(1–3), 103–127. https://doi.org/10.1016/0031-0182(81)90034-1

Dickson, A. G., Sabine, C. L., Christian, J. R., & Bargeron, C. P. (2007). North Pacific marine science organization. In *Guide to best practices for ocean CO_2 measurements*. PICES special publication. North Pacific Marine Science Organization.

Dietzel, M., Purgstaller, B., Kluge, T., Leis, A., & Mavromatis, V. (2020). Oxygen and clumped isotope fractionation during the formation of Mg calcite via an amorphous precursor. *Geochimica et Cosmochimica Acta*, *276*, 258–273. https://doi.org/10.1016/j.gca.2020.02.032

Dietzel, M., Tang, J., Leis, A., & Köhler, S. J. (2009). Oxygen isotopic fractionation during inorganic calcite precipitation——Effects of temperature, precipitation rate and pH. *Chemical Geology*, *268*(1–2), 107–115. https://doi.org/10.1016/j.chemgeo.2009.07.015

Dimarchopoulou, D., Keramidas, I., Tsagarakis, K., Markantonatou, V., Halouani, G., & Tsikliras, A. C. (2024). Spatiotemporal fishing effort simulations and restriction scenarios in Thermaikos Gulf, Greece (northeastern Mediterranean Sea). *Ocean & Coastal Management*, *247*, 106914. https://doi.org/10.1016/j.ocecoaman.2023.106914

Fabry, V. J., & Deuser, W. G. (1991). Aragonite and magnesian calcite fluxes to the deep Sargasso Sea. *Deep-Sea Research, Part A: Oceanographic Research Papers*, *38*(6), 713–728. https://doi.org/10.1016/0198-0149(91)90008-4

Fabry, V. J., & Deuser, W. G. (1992). Seasonal changes in the isotopic compositions and sinking fluxes of euthecosomatous pteropod shells in the Sargasso Sea. *Paleoceanography*, *7*(2), 195–213. https://doi.org/10.1029/91pa03138

Folkerts, E. J., Oehlert, A. M., Heuer, R. M., Nixon, S., Stieglitz, J. D., & Grosell, M. (2024). The role of marine fish-produced carbonates in the oceanic carbon cycle is determined by size, specific gravity, and dissolution rate. *Science of the Total Environment*, *916*, 170044. https://doi.org/10.1016/j.scitotenv.2024.170044

Gabitov, R. I., Watson, E. B., & Sadekov, A. (2012). Oxygen isotope fractionation between calcite and fluid as a function of growth rate and temperature: An in situ study. *Chemical Geology*, *306–307*, 92–102. https://doi.org/10.1016/j.chemgeo.2012.02.021

García-Charton, J. A., Pérez-Ruzafa, Á., Sánchez-Jerez, P., Bayle-Sempere, J. T., Reñones, O., & Moreno, D. (2004). Multi-scale spatial heterogeneity, habitat structure, and the effect of marine reserves on Western Mediterranean rocky reef fish assemblages. *Marine Biology*, *144*(1), 161–182. https://doi.org/10.1007/s00227-003-1170-0

Ghilardi, M., Salter, M. A., Parravicini, V., Ferse, S. C. A., Rixen, T., Wild, C., et al. (2023). Temperature, species identity and morphological traits predict carbonate excretion and mineralogy in tropical reef fishes. *Nature Communications*, *14*(1), 985. https://doi.org/10.1038/s41467-023-36617-7

Gray. (2019). *Environmental controls on Helicondoides sp. and Styliola sp. Pteropod shell flux and isotopic composition in the Sargasso Sea*. University of Massachusetts Dartmouth.

Grosell, M. (2019). CO_2 and calcification processes in fish. In *Fish physiology* (pp. 133–159). Elsevier.

Grosell, M., & Oehlert, A. M. (2023). Staying hydrated in seawater. *Physiology*, *38*(4), 178–188. https://doi.org/10.1152/physiol.00005.2023

Hashim, M., Conte, M. H., Salter, M. A., Pedrosa Pàmies, R., Weber, J., Hayden, M. G., et al. (2025a). Presence and abundance of blue particles in Oceanic Flux Program (OFP) samples collected from 1984–2019 at the OFP mooring in the Sargasso Sea Biological and Chemical Oceanography Data Management Office (BCO-DMO). (Version 1) version date 2025-05-06 [dataset]. https://doi.org/10.26008/1912/bco-dmo.960203.1

Hashim, M., Conte, M. H., Salter, M. A., Pedrosa Pàmies, R., Weber, J., Hayden, M. G., et al. (2025b). Metadata (location, depth, water temperature, salinity, etc.) describing end members compared to blue particles found in Oceanic Flux Program (OFP) traps. Biological and Chemical Oceanography Data Management Office (BCO-DMO). (Version 1) Version Date 2025-05-07 [dataset]. https://doi.org/10.26008/1912/bco-dmo.960257.1

Hashim, M., Conte, M. H., Salter, M. A., Pedrosa Pàmies, R., Weber, J., Hayden, M. G., et al. (2025c). A compilation of newly measured as well as compiled d13C and d18O of carbonates for various types of samples. Biological and Chemical Oceanography Data Management Office (BCO-DMO). (Version 1) Version Date 2025-05-14 [dataset]. https://doi.org/10.26008/1912/bco-dmo.960397.1

Hashim, M., Conte, M. H., Salter, M. A., Pedrosa Pàmies, R., Weber, J., Hayden, M. G., et al. (2025d). Results of x-ray diffraction (XRD) analyses collected for various Oceanic Flux Program (OFP) samples and end members for the for OFP/fish carbonate study. Biological and Chemical Oceanography Data Management Office (BCO-DMO). (Version 1) version date 2025-05-08 [dataset]. https://doi.org/10.26008/1912/bco-dmo.960297.1

Hashim, M. S., Burke, J. E., Hardisty, D. S., & Kaczmarek, S. E. (2022). Iodine incorporation into dolomite: Experimental constraints and implications for the iodine redox proxy and Proterozoic Ocean. *Geochimica et Cosmochimica Acta*, *338*, 365–381. https://doi.org/10.1016/j.gca.2022.10.027

Hashim, M. S., & Kaczmarek, S. E. (2019). A review of the nature and origin of limestone microporosity. *Marine and Petroleum Geology*, *107*, 527–554. https://doi.org/10.1016/j.marpetgeo.2019.03.037

Hashim, M. S., & Kaczmarek, S. E. (2020). Experimental stabilization of carbonate sediments to calcite: Insights into the depositional and diagenetic controls on calcite microcrystal texture. *Earth and Planetary Science Letters*, *538*, 116235. https://doi.org/10.1016/j.epsl.2020.116235

Hashim, M. S., & Kaczmarek, S. E. (2021). The transformation of aragonite to calcite in the presence of magnesium: Implications for marine diagenesis. *Earth and Planetary Science Letters*, *574*, 117166. https://doi.org/10.1016/j.epsl.2021.117166

Hashim, M. S., & Kaczmarek, S. E. (2022). Rhombic calcite microcrystals as a textural proxy for meteoric diagenesis. *Scientific Reports*, *12*(1), 213. https://doi.org/10.1038/s41598-021-04219-2

Hashim, M. S., Kaczmarek, S. E., Wolfram Naa, G., Bish, D. L., & Subhas, A. V. (2024). A process-based geochemical framework for carbonate sediments during marine diagenesis. *Geochimica et Cosmochimica Acta*, *376*, 54–67. https://doi.org/10.1016/j.gca.2024.05.023

Hashim, M. S., Rose, K. G., Cohen, H. F., & Kaczmarek, S. E. (2023). Effects of sodium and potassium concentrations on dolomite formation rate, stoichiometry and crystallographic characteristics. *Sedimentology*, *70*(7), 2355–2370. https://doi.org/10.1111/sed.13124

Hermoso, M., Horner, T. J., Minoletti, F., & Rickaby, R. E. M. (2014). Constraints on the vital effect in coccolithophore and dinoflagellate calcite by oxygen isotopic modification of seawater. *Geochimica et Cosmochimica Acta*, *141*, 612–627. https://doi.org/10.1016/j.gca.2014.05.002

Irigoien, X., Klevjer, T. A., Røstad, A., Martinez, U., Boyra, G., Acuña, J. L., et al. (2014). Large mesopelagic fishes biomass and trophic efficiency in the open ocean. *Nature Communications*, *5*(1), 3271. https://doi.org/10.1038/ncomms4271

Jasper, J. P., & Deuser, W. G. (1993). Annual cycles of mass flux and isotopic composition of pteropod shells settling into the deep Sargasso Sea. *Deep Sea Research Part I: Oceanographic Research Papers*, *40*(4), 653–669. https://doi.org/10.1016/0967-0637(93)90064-A

Jennings, S., & Collingridge, K. (2015). Predicting consumer biomass, size-structure, production, catch potential, responses to fishing and associated uncertainties in the world's marine ecosystems. *PLoS One*, *10*(7), e0133794. https://doi.org/10.1371/journal.pone.0133794

Jiménez-López, C., Romanek, C. S., Huertas, F. J., Ohmoto, H., & Caballero, E. (2004). Oxygen isotope fractionation in synthetic magnesian calcite 1. *Geochimica et Cosmochimica Acta*, *68*(16), 3367–3377. https://doi.org/10.1016/j.gca.2003.11.033

Juranek, L. W., Russell, A. D., & Spero, H. J. (2003). Seasonal oxygen and carbon isotope variability in euthecosomatous pteropods from the Sargasso Sea. *Deep Sea Research Part I: Oceanographic Research Papers*, *50*(2), 231–245. https://doi.org/10.1016/S0967-0637(02)00164-4

Keeling, C. D., Brix, H., & Gruber, N. (2004). Seasonal and long-term dynamics of the upper ocean carbon cycle at Station ALOHA near Hawaii. *Global Biogeochemical Cycles*, *18*(4). https://doi.org/10.1029/2004GB002227

Kieckbusch, D., Koch, M., Serafy, J., & Anderson, W. (2004). Trophic linkages among primary producers and consumers in fringing mangroves of subtropical lagoons. *Bulletin of Marine Science*, *74*, 271–285.

Kim, S.-T., & O'Neil, J. R. (1997). Equilibrium and nonequilibrium oxygen isotope effects in synthetic carbonates. *Geochimica et Cosmochimica Acta*, *61*(16), 3461–3475. https://doi.org/10.1016/S0016-7037(97)00169-5

Knecht, N. S., Benedetti, F., Hofmann Elizondo, U., Bednaršek, N., Chaabane, S., De Weerd, C., et al. (2023). The impact of zooplankton calcifiers on the marine carbon cycle. *Global Biogeochemical Cycles*, *37*(6), e2022GB007685. https://doi.org/10.1029/2022GB007685

Kwon, E. Y., Dunne, J. P., & Lee, K. (2024). Biological export production controls upper ocean calcium carbonate dissolution and CO_2 buffer capacity. *Science Advances*, *10*(13), eadl0779. https://doi.org/10.1126/sciadv.adl0779

Lamb, K., Swart, P. K., & Altabet, M. A. (2012). Nitrogen and carbon isotopic systematics of the Florida reef tract. *Bulletin of Marine Science*, *88*(1), 119–146. https://doi.org/10.5343/bms.2010.1105

Langer, M. R. (2008). Assessing the contribution of Foraminiferan Protists to global ocean carbonate production1. *The Journal of Eukaryotic Microbiology*, *55*(3), 163–169. https://doi.org/10.1111/j.1550-7408.2008.00321.x

Liang, H., Lunstrum, A. M., Dong, S., Berelson, W. M., & John, S. G. (2023). Constraining CaCO3 export and dissolution with an ocean alkalinity inverse model. *Global Biogeochemical Cycles*, *37*(2), e2022GB007535. https://doi.org/10.1029/2022GB007535

Lomas, M. W., Bates, N. R., Johnson, R. J., Knap, A. H., Steinberg, D. K., & Carlson, C. A. (2013). Two decades and counting: 24-years of sustained open ocean biogeochemical measurements in the Sargasso Sea. *Deep Sea Research Part II: Topical Studies in Oceanography, Measuring Ocean Change: Results from BATS, HOT, and CARIACO*, *93*, 16–32. https://doi.org/10.1016/j.dsr2.2013.01.008

Mavromatis, V., Schmidt, M., Botz, R., Comas-Bru, L., & Oelkers, E. H. (2012). Experimental quantification of the effect of Mg on calcite–aqueous fluid oxygen isotope fractionation. *Chemical Geology*, *310–311*, 97–105. https://doi.org/10.1016/j.chemgeo.2012.03.027

McConnaughey, T. (1989a). ^{13}C and ^{18}O isotopic disequilibrium in biological carbonates: I. Patterns. *Geochimica et Cosmochimica Acta*, *53*(1), 151–162. https://doi.org/10.1016/0016-7037(89)90282-2

McConnaughey, T. (1989b). ^{13}C and ^{18}O isotopic disequilibrium in biological carbonates: II. In vitro simulation of kinetic isotope effects. *Geochimica et Cosmochimica Acta*, *53*(1), 163–171. https://doi.org/10.1016/0016-7037(89)90283-4

McConnaughey, T. A., Burdett, J., Whelan, J. F., & Paull, C. K. (1997). Carbon isotopes in biological carbonates: Respiration and photosynthesis. *Geochimica et Cosmochimica Acta*, *61*(3), 611–622. https://doi.org/10.1016/S0016-7037(96)00361-4

McCrea, J. M. (1950). On the isotopic chemistry of carbonates and a paleotemperature scale. *The Journal of Chemical Physics*, *18*(6), 849–857. https://doi.org/10.1063/1.1747785

Milliman, J. D. (1993). Production and accumulation of calcium carbonate in the ocean: Budget of a nonsteady state. *Global Biogeochemical Cycles*, *7*(4), 927–957. https://doi.org/10.1029/93GB02524

Milliman, J. D., & Droxler, A. W. (1996). Neritic and pelagic carbonate sedimentation in the marine environment: Ignorance is not bliss 9.

Morse, J. W., Andersson, A. J., & Mackenzie, F. T. (2006). Initial responses of carbonate-rich shelf sediments to rising atmospheric pCO2 and "ocean acidification": Role of high Mg-calcites. *Geochimica et Cosmochimica Acta*, *70*(23), 5814–5830. https://doi.org/10.1016/j.gca.2006.08.017

Morse, J. W., Arvidson, R. S., & Lüttge, A. (2007). Calcium carbonate formation and dissolution. *Chemical Reviews*, *107*(2), 342–381. https://doi.org/10.1021/cr050358j

Mucci, A. (1983). The solubility of calcite and aragonite in seawater at various salinities, temperatures, and one atmosphere total pressure. *American Journal of Science*, *283*(7), 780–799. https://doi.org/10.2475/ajs.283.7.780

Neukermans, G., Bach, L. T., Butterley, A., Sun, Q., Claustre, H., & Fournier, G. R. (2023). Quantitative and mechanistic understanding of the open ocean carbonate pump—Perspectives for remote sensing and autonomous in situ observation. *Earth-Science Reviews*, *239*, 104359. https://doi.org/10.1016/j.earscirev.2023.104359

Oehlert, A. M., Arista, K., Folkerts, E., Walls, S., Garza, J., Vitek, B., et al. (2024). Organic coatings reduce mineral dissolution rate of sinking ichthyocarbonate by an order of magnitude. In *2024 ocean Sciences Meeting*. AGU.

Oehlert, A. M., Garza, J., Nixon, S., Frank, L., Folkerts, E. J., Stieglitz, J. D., et al. (2024). Implications of dietary carbon incorporation in fish carbonates for the global carbon cycle. *Science of the Total Environment*, *916*, 169895. https://doi.org/10.1016/j.scitotenv.2024.169895

Ostermann, D. R., & Curry, W. B. (2000). Calibration of stable isotopic data: An enriched $\delta^{18}O$ standard used for source gas mixing detection and correction. *Paleoceanography*, *15*(3), 353–360. https://doi.org/10.1029/1999PA000411

Pedrosa-Pamies, R., Conte, M. H., Weber, J. C., & Andersson, A. J. (2025). Hurricane-driven transport of Bermuda reef carbonate platform sediments to the deep ocean. *Journal of Geophysical Research: Oceans*, *130*(3), e2023JC020500. https://doi.org/10.1029/2023JC020500

Perry, C. T., Salter, M. A., Harborne, A. R., Crowley, S. F., Jelks, H. L., & Wilson, R. W. (2011). Fish as major carbonate mud producers and missing components of the tropical carbonate factory. *Proceedings of the National Academy of Sciences of the United States of America*, *108*(10), 3865–3869. https://doi.org/10.1073/pnas.1015895108

Proud, R., Handegard, N. O., Kloser, R. J., Cox, M. J., & Brierley, A. S. (2019). From siphonophores to deep scattering layers: Uncertainty ranges for the estimation of global mesopelagic fish biomass. *ICES Journal of Marine Science*, *76*(3), 718–733. https://doi.org/10.1093/icesjms/fsy037

Ralph, N., Conte, M. H., Turner, J., Arnold, E., & Manganini, S. (1998). Enigmatic blue aggregates of submicron size carbonate particles in the Sargasso Sea. *Eos, Transactions American Geophysical Union*, *79*, OS9.

Ridgwell, A. J., Watson, A. J., Maslin, M. A., & Kaplan, J. O. (2003). Implications of coral reef buildup for the controls on atmospheric CO_2 since the Last Glacial Maximum. *Paleoceanography*, *18*(4). https://doi.org/10.1029/2003PA000893

Salter, M. A., Harborne, A. R., Perry, C. T., & Wilson, R. W. (2017). Phase heterogeneity in carbonate production by marine fish influences their roles in sediment generation and the inorganic carbon cycle. *Scientific Reports*, *7*(1), 765. https://doi.org/10.1038/s41598-017-00787-4

Salter, M. A., Perry, C. T., & Smith, A. M. (2019). Calcium carbonate production by fish in temperate marine environments. *Limnology & Oceanography*, *64*(6), 2755–2770. https://doi.org/10.1002/lno.11339

Salter, M. A., Perry, C. T., Stuart-Smith, R. D., Edgar, G. J., Wilson, R. W., & Harborne, A. R. (2018). Reef fish carbonate production assessments highlight regional variation in sedimentary significance. *Geology*, *46*(8), 699–702. https://doi.org/10.1130/G45286.1

Salter, M. A., Perry, C. T., & Wilson, R. W. (2012). Production of mud-grade carbonates by marine fish: Crystalline products and their sedimentary significance. *Sedimentology*, *59*(7), 2172–2198. https://doi.org/10.1111/j.1365-3091.2012.01339.x

Salter, M. A., Perry, C. T., & Wilson, R. W. (2014). Size fraction analysis of fish-derived carbonates in shallow sub-tropical marine environments and a potentially unrecognised origin for peloidal carbonates. *Sedimentary Geology*, *314*, 17–30. https://doi.org/10.1016/j.sedgeo.2014.10.005

Schlitzer, R. (2022). Ocean data view. Retrieved from https://odv.awi.de

Shatova, O., Koweek, D., Conte, M. H., & Weber, J. C. (2012). Contribution of zooplankton fecal pellets to deep ocean particle flux in the Sargasso Sea assessed using quantitative image analysis. *Journal of Plankton Research*, *34*(10), 905–921. https://doi.org/10.1093/plankt/fbs053

Siegel, D. A., & Armstrong, R. A. (2002). Corrigendum to "trajectories of sinking particles in the Sargasso Sea: Modeling of statistical funnels above deep-ocean sediment traps". *Deep-Sea Research Part I*, *6*, 1115–1116.

Steiger. (2019). Seasonal and intra-annual variability in shell chemistry of planktonic foraminifera Globigerinoides ruber (white) morphotypes in the Sargasso Sea: 1998-2010. *UMass Dartmouth*.

Su, J., Cai, W.-J., Hussain, N., Brodeur, J., Chen, B., & Huang, K. (2019). Simultaneous determination of dissolved inorganic carbon (DIC) concentration and stable isotope ($\delta^{13}C$-DIC) by Cavity Ring-Down Spectroscopy: Application to study carbonate dynamics in the Chesapeake Bay. *Marine Chemistry*, *215*, 103689. https://doi.org/10.1016/j.marchem.2019.103689

Subhas, A. V., Dong, S., Naviaux, J. D., Rollins, N. E., Ziveri, P., Gray, W., et al. (2022). Shallow calcium carbonate cycling in the North Pacific Ocean. *Global Biogeochemical Cycles*, *36*(5). https://doi.org/10.1029/2022GB007388

Subhas, A. V., McCorkle, D. C., Quizon, A., McNichol, A. P., & Long, M. H. (2019). Selective preservation of coccolith calcite in Ontong-Java plateau sediments. *Paleoceanography and Paleoclimatology*, *34*(12), 2141–2157. https://doi.org/10.1029/2019pa003731

Sulpis, O., Jeansson, E., Dinauer, A., Lauvset, S. K., & Middelburg, J. J. (2021). Calcium carbonate dissolution patterns in the ocean. *Nature Geoscience*, *14*(6), 423–428. https://doi.org/10.1038/s41561-021-00743-y

Tarutani, T., Clayton, R. N., & Mayeda, T. K. (1969). The effect of polymorphism and magnesium substitution on oxygen isotope fractionation between calcium carbonate and water. *Geochimica et Cosmochimica Acta*, *33*(8), 987–996. https://doi.org/10.1016/0016-7037(69)90108-2

Thayer, G. W., Govoni, J. J., & Connally, D. W. (1983). Stable carbon isotope ratios of the planktonic food web in the northern Gulf of Mexico. *Bulletin of Marine Science*, *33*, 247–256.

Walsh, P. J., Blackwelder, P., Gill, K. A., Danulat, E., & Mommsen, T. P. (1991). Carbonate deposits in marine fish intestines: A new source of biomineralization. *Limnology & Oceanography*, *36*(6), 1227–1232. https://doi.org/10.4319/lo.1991.36.6.1227

Watkins, J. M., Hunt, J. D., Ryerson, F. J., & DePaolo, D. J. (2014). The influence of temperature, pH, and growth rate on the $\delta^{18}O$ composition of inorganically precipitated calcite. *Earth and Planetary Science Letters*, *404*, 332–343. https://doi.org/10.1016/j.epsl.2014.07.036

Watkins, J. M., Nielsen, L. C., Ryerson, F. J., & DePaolo, D. J. (2013). The influence of kinetics on the oxygen isotope composition of calcium carbonate. *Earth and Planetary Science Letters*, *375*, 349–360. https://doi.org/10.1016/j.epsl.2013.05.054

Watson, E. B. (2004). A conceptual model for near-surface kinetic controls on the trace-element and stable isotope composition of abiogenic calcite crystals. *Geochimica et Cosmochimica Acta*, *68*(7), 1473–1488. https://doi.org/10.1016/j.gca.2003.10.003

White, M. M., Waller, J. D., Lubelczyk, L. C., Drapeau, D. T., Bowler, B. C., Balch, W. M., & Fields, D. M. (2018). Coccolith dissolution within copepod guts affects fecal pellet density and sinking rate. *Scientific Reports*, *8*(1), 9758. https://doi.org/10.1038/s41598-018-28073-x

Whitworth, T. M., Mariñas, B. J., & Fritz, S. J. (1994). Isotopic fractionation and overall permeation of lithium by a thin-film composite polyamide reverse osmosis membrane. *Journal of Membrane Science*, *88*(2–3), 231–241. https://doi.org/10.1016/0376-7388(94)87009-8

Wilson, R. W., Millero, F. J., Taylor, J. R., Walsh, P. J., Christensen, V., Jennings, S., & Grosell, M. (2009). Contribution of fish to the marine inorganic carbon cycle. *Science*, *323*(5912), 359–362. https://doi.org/10.1126/science.1157972

Wilson, R. W., Wilson, J. M., & Grosell, M. (2002). Intestinal bicarbonate secretion by marine teleost fish—Why and how? Biochimica et Biophysica Acta (BBA)—Biomembranes, Epithelial Ion Transport-A Tribute to Hans H. *Ussing*, *1566*(1–2), 182–193. https://doi.org/10.1016/S0005-2736(02)00600-4

Woosley, R. J., Millero, F. J., & Grosell, M. (2012). The solubility of fish-produced high magnesium calcite in seawater: Solubility of fish-produced mg calcite. *Journal of Geophysical Research*, *117*(C4). https://doi.org/10.1029/2011JC007599

Zhang, F., Xu, H., Konishi, H., & Roden, E. E. (2010). A relationship between d 104 value and composition in the calcite-disordered dolomite solid-solution series. *American Mineralogist*, *95*(11–12), 1650–1656. https://doi.org/10.2138/am.2010.3414

Ziveri, P., Gray, W. R., Anglada-Ortiz, G., Manno, C., Grelaud, M., Incarbona, A., et al. (2023). Pelagic calcium carbonate production and shallow dissolution in the North Pacific Ocean. *Nature Communications*, *14*(1), 805. https://doi.org/10.1038/s41467-023-36177-w